Volume 15, Issue 4, 152426 (1-31)

International Journal of Nano Dimension (IJND)

https://dx.doi.org/10.57647/j.ijnd.2024.1504.26

Nanostructured carbon dots as ratiometric fluorescent rulers for heavy metal detection

Venkatakrishnan Kiran, Karthick Harini, Anbazhagan Thirumalai, Koyeli Girigoswami, Agnishwar Girigoswami*

Medical Bionanotechnology, Faculty of Allied Health Sciences, Chettinad Hospital & Research Institute (CHRI), Chettinad Academy of Research and Education (CARE), Kelambakkam, Chennai, India.

***Corresponding author:** agnishwarg@gmail.com

Review Paper

Received:
06 April 2024
Revised:
04 July 2024
Accepted:
10 July 2024
Published online:
10 October 2024

Abstract:

Carbon dots (CDs) have garnered significant attention in heavy metal (HM) sensing due to their exceptional optical properties and numerous advantages. Due to the rapid industrialization in the last couple of decades, the accumulation of HM in the environment poses a major threat to humans and marine and terrestrial organisms in the Indian subcontinent. Therefore, the detection of HM in the environment is of paramount importance. This review delineates the latest progress in employing CDs for heavy metal detection, specifically focusing on those with dual-emissive fluorescence characteristics, highlighting their superiority compared to traditional detection approaches. Additionally, eco-friendly synthesis methods and the mechanisms through which heavy metals are sensed by CDs are investigated, with emphasis placed on their benefits, such as high sensitivity and selectivity in metal detection applications. The review examines a variety of detection methods employing CDs, such as fluorescence, colorimetry, electrochemical techniques sensing, and ratiometric fluorescence methods, and elucidates their distinct applications. Furthermore, it focuses on approaches aimed at enhancing the sensing capabilities of CDs through surface functionalization, doping, and composite formation. By providing a comprehensive overview of detection methods and suggesting avenues for further research and development, it aims to contribute to the advancement of this field.

Keywords: Carbon dots; Fluorescence; Heavy metals; Ratiometric sensing; Sensor

1. Introduction

Metals that have a density greater than 5 g/cm^3 are classified as heavy metals. These elements, which have high atomic weights and densities, are naturally occurring in the Earth's crust. Heavy metals are divided into two main categories: essential and nonessential. Essential heavy metals are vital for various biological functions, including growth, metabolism, and the development of organs in living beings. For instance, Cu, Fe, Mn, Co, Zn, Ni, and others are considered essential as they act as cofactors that are critical for the structural integrity and activity of enzymes and proteins in both animals and plants. These vital metals are needed only in small amounts and are often referred to as trace elements or micronutrients. On the other hand, nonessential heavy metals like Cd, Pb, Hg, Cr, Al, and others do not play any known beneficial role in metabolic processes, even in minute amounts. [1]. Due to the rapid growth of industries such as chrome plating, leather tanning industry, pesticides and herbicide manufacturing, pharmaceutical industry, and battery manufacturing, the sources of heavy metals in soil and marine regions increased rapidly [2]. HMs are considered to be toxic to humans and marine organisms due to bio-accumulation. HMs in the environment can reach the human body through several routes, especially dermal or inhalation routes or drinking heavy metal-contaminated water and food. They produce various modes of toxicities in human bodies, such as genotoxicity, neurotoxicity, hepatotoxicity, carcinogenicity, skin toxicity, etc (Figure 1). Requisite elements in the body are replaced by HMs if continuously exposed to HMs from the environment [3]. Detecting heavy metals in soil and water before

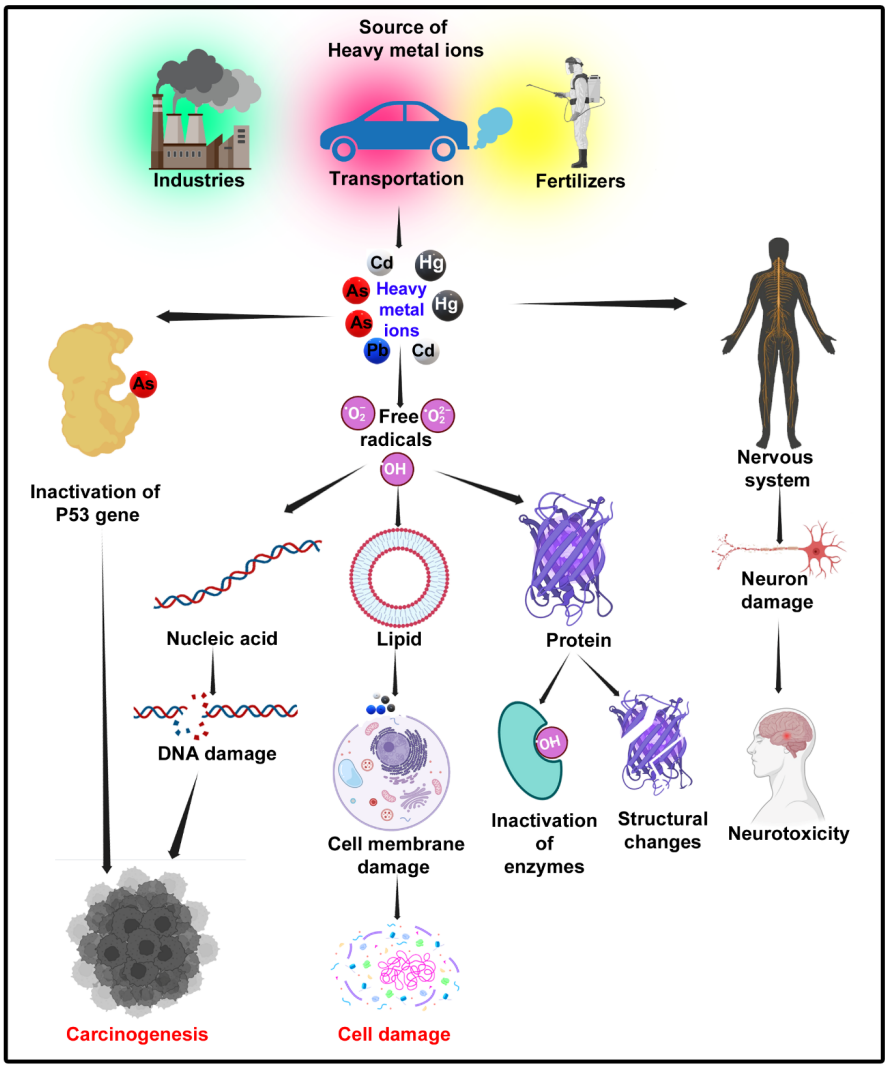

Figure 1. Mechanism of heavy metal toxicity in humans.

their use has become imperative due to the array of issues stemming from their improper release into the environment by industries without adequate remediation measures. The World Health Organization (WHO) has established minimum concentration levels (MCL) for heavy metals in soil and water, underlining the critical importance of monitoring and adhering to these guidelines.

The increased level of HMs needs to be detected earlier and removed to prevent any health hazard. Therefore, the detection of heavy HMs holds significant importance in environmental monitoring. It enables the assessment of contamination levels and potential risks to both ecosystems and human health. Through precise identification and measurement of hazardous substances, proactive measures can be implemented to mitigate their impact and safeguard the environment, ensuring its preservation and protection. Detection of HMs can be performed by methods such as Atomic absorption spectroscopy (AAS), Inductively coupled plasma optical mass spectroscopy (ICP-MS), Hybrid generation atomic absorption spectroscopy (HG-AAS), and High-performance liquid chromatography (HPLC). Even though these methods can be afforded to detect HMs in trace levels with high sensitivity and accuracy, they possess some disadvantages, such as time consumption, cost, and complication in instrumentation, as they require expertized persons to handle [4]. Hence, to overcome these disadvantages of conventional methods, researchers have developed nanomaterials (NMs) -based sensors for the detection of HMs in the environment. NMs such as metal nanoparticles, silica nanoparticles, metal-organic frameworks (MOFs), and carbon dots (CDs) are the most frequently used particles in detecting HMs. But, among these, CDs are widely used because of ease of functionalization, stability under various environmental conditions, tunable properties, high sensitivity, and selectivity [5, 6]. The ratiometric sensing method utilizes a fluorescent probe with two emission (EM) wavelengths under a single excitation wavelength for effectively sensing HMs without interference from background noise, instrument error, environmental changes, and sensor concentration variation. CDs are doped/hybridized with other luminescent materials for effectively sensing HMs with two EM peaks under a single excitation wavelength [7]. This review discussed the role of CDs in detecting various HMs through fluorescence, colorimetric, electrochemical, and

ratiometric sensing methods. With the advantages of ratiometric sensing over fluorescence (FL) and colorimetric sensing, recent research investigations have been compiled to provide detailed insight into the topic.

To date, CDs have been synthesized from various precursors, yet researchers continue to seek appropriate precursors to tune luminescence, which is often hindered by passivating factors and toxic chemicals. Natural or renewable resource-generated fluorescent CDs have been synthesized using a variety of bottom-up approaches, including hydrothermal or solvothermal methods, microwave irradiation, ultrasonic techniques, and thermal decomposition [8–10]. Green synthesis methods facilitate CD fabrication by minimizing the use of toxic and carcinogenic solvents. Various natural resources, such as crab shells, prawn shells, green tea leaves, coffee, garlic, ginger, and bio-wastes, have been used as carbon sources to develop fluorescent CDs, thereby overcoming surface passivation [11, 12]. Therefore, the successful fabrication of CDs is achievable through the careful selection of precursors with significant physical and biological properties combined with green synthesis approaches. This review also emphasizes the role of green route synthesized CDs in sensing mechanisms.

2. A threat from heavy metals: India's perspective

India's major HM toxicity includes arsenic, mercury, lead, iron, and chromium. The two major water resources of India, the Ganges and Yamuna Rivers, are contaminated with HM pollutants. Arsenic is derived from various sources, including domestic, industrial, and electronic waste, agricultural activities, as well as improper disposal and mishandling of solid waste. The government imposed several measures for the prevention of arsenic contamination. The plans are categorized into defensive and proactive methods. The defensive tactics encompass various actions, including scientific gathering, purification, proper disposal of arsenic-contaminated water, on-site management of industrial wastewater, and the control of chemical fertilizers, pesticides, and insecticide usage. The proactive methods include creating awareness among the Indian masses and the unconcerned public, creating artificial lakes to store the flood waters, and releasing it in the Yamuna River during the dry period [13]. The Ganga River, stretching 2525 km from Gangotri to the Bay of Bengal, covers an expansive area of 8,61.404 km^2 and serves as a crucial water source for the Indian population. The states such as Uttarakhand, Uttar Pradesh, Bihar, Jharkhand, and West Bengal are the states in which the Ganga River flows are heavily contaminated by Industrial wastewater. The CPCB monitors the stretch of the Ganga River from Rishikesh to Varanasi, with the central portion spanning Kannauj to Kanpur and Varanasi being identified as the most polluted segment [14]. The 2023 reports from the Central Pollution Control Board (CPCB) on the Ganga River highlight a slight surpassing of permissible Biochemical Oxygen Demand (BOD) levels. Specifically, BOD levels range from 3.2 to 4.5 mg/L between Farrukhabad and Varanasi, indicating a minor breach of acceptable thresholds. BOD measures the dissolved oxygen required by microorganisms to decompose organic substances in water. Higher BOD levels indicate increased organic pollution, posing risks of oxygen depletion and harm to aquatic ecosystems. Thus, these findings emphasize the need for ongoing scientific monitoring and coordinated actions to address pollution across the Ganga River basin, ensuring its ecological well-being and long-term sustainability.

2.1 Cadmium (Cd)

Cd is a pliable metal often considered toxic because of its unknown physiological functions in humans and organisms [15]. Cd has a half-life of $16-30$ years in the human body and varies in concentration throughout the body. Cd is discharged into the environment through human activities such as industries of Ni-Cd batteries, corrosive agents, and plasticizers in PVC products. Smoking habit of humans also increases the Cd concentration in blood and urine. People working in industries of glass production, alloys, electroplating, and batteries are frequently exposed and have chronic disabilities. International Agency for Research on Cancer (IRAC) classified Cd as a carcinogen (Group 1). Natural activities such as volcanic erosion, abrasion of soil and rocks, forest fires, and mines of zinc, lead, and arsenic are also contributors to Cd in the atmosphere, soil, and water. Cd enters the human body through the respiratory tract and also, a small amount through the gastrointestinal tract but skin absorption of Cd is extremely rare [16]. Once Cd is absorbed into the body erythrocytes and albumin facilitate in transport of them to the bloodstream and accumulate them in the liver, kidney, and gut. Cd is excreted from the human body through means of urine, saliva, and milk during lactation. Intake of Cd-contaminated foods also results in various problems [17]. In 2013, researchers from University of Kalyani conducted a study to evaluate the exposure of Cd effects on workers of small-scale jewellers in Kolkata with a sample size of 133 individuals [18]. Results showed that workers had 10 times higher Cd concentration ($2.74-9.89$ μg/dl) in urine excretion when compared to the jewellers shop salesman ($0.18-0.78$ μg/dl). Goyal et al. conducted a study in Jodhpur, Rajasthan composed of 207 individuals, grouped into 110 working in industries (test group) and 97 individuals (control group) to evaluate the lead and cadmium levels in the blood [19]. The exposed individuals had a cadmium level of $0.16-7.00$ whereas the control group had $0.02-3.96$ μg/l, in the case of lead, the test group had $0.34-114.2$ μg/dl, and the control group had $0.04-2.98$ μg/dl.

2.2 Mercury

Mercury, a common HM pollutant with unknown function in physiology and human biochemistry, has three different forms: elemental, organic, and inorganic. While mercury exists in minimal quantities in the environment, its toxic nature, long-lasting effects, and tendency to accumulate in organisms continue to significantly affect both humans and other living beings. Mercury undergoes oxidation, transforming into vapor form, which then enters the respiratory system due to its inability to pass through the gastrointestinal tract. In red blood cells and tissues, hydrogen peroxide and peroxidise oxidize the elemental mercury into inor-

ganic mercury because of their soluble property. Inorganic mercury leads to autoimmune diseases and antinuclear antibodies in exposed individuals [20]. Mercury exposure also leads to increased production of free radicals, ROS, and superoxide anions due to Fenton reactions [21]. $HgCl_2$ is an important form of mercury known for its organotoxic and carcinogenic properties. $HgCl_2$, in the past decade, has been widely used as an ingredient in skin whitening creams for the removal of freckles and dark spots on the skin that occur because of melanin accumulation. Hg^0, a form of mercury, can penetrate through the blood-brain barrier (BBB) and placenta and produce toxicity. Organic Hg can enter the gastrointestinal tract and is easily distributed in the body [22].

2.3 Arsenic

Arsenic is considered a major HM contamination source in the Indian scenario. A study revealed an increasing concentration of arsenic in the Gangetic Plain, Bihar [23]. In the states of UP, the arsenic range was observed between $2.0 - 1310$ ppb, but most of the samples contain arsenic in the range of 0.5 mg/L, which is considered to be an admissible value of arsenic in drinking water. In 1983, India first reported arsenic contamination in West Bengal's drinking water. Organic forms of arsenic such as arsenic trioxide, arsenopyrite, orpiment, and realgar are carcinogenic to humans. Arsenic is also known to be proto-plastic poison, which results in abnormal cell respiration, cell enzyme degradation, and mitosis by first attacking the sulfhydryl group of cells. Accidental consumption and suicidal attempts based on arsenic lead to acute poisoning [24]. Acute poisoning may also be caused by the intake of pesticide-contaminated foods, arsenic-rich foods, or arsenic soils [25]. Acute poisoning of arsenic also happens through drinking adulterated milk, which contains a source of arsenic water. Short exposure to arsenic poisoning results in vomiting, muscle pain, numbness, diarrhea, changes in the normal heartbeat and, whereas long-term exposure to inorganic arsenic leads to skin irritation, pigmentation, skin lesions, and patches in the palm, and extreme conditions lead to skin cancer, tumor in kidneys, lungs, bladder, and liver [26]. The arsenic mechanism of toxicity is much more complex because it involves five major metabolites, all of which can cause toxic effects [27]. The liver metabolizes the inorganic trivalent arsenic, which involves the successive reductive methylation by the enzyme arsenic methyltransferase (AS3MT) in the presence of the cofactors glutathione (GSH) and S-adenosylmethionine (SAM), resulting in the formation of protein-bound intermediate metabolites such as monomethylarsonous acid [MMA] (V) and dimethylarsinous acid [DMA]. These intermediates are further oxidized to less toxic pentavalent forms, MMA (V) and DMA (V), before being excreted in the urine [28].

2.4 Lead

Lead is an HM with a low melting point and bluish-grey color in appearance, feasible to mold into any shape, and can easily form an alloy with other metals. Continued exposure to lead in males leads to impotence, while in pregnant women, it causes miscarriage [29]. Over-dosage of lead molecules in the blood causes neurological, cardiovascular, hematologic, and reproductive problems. The mechanism of lead-driven toxicity is that lead at the cellular level binds to the sulfhydryl group of GSH and blocks the activity of some enzymes, which causes reduced GSH levels, further resulting in the instability of cellular membrane through lipid peroxidation, which may be led to hemolytic anemia [30]. Lead can easily influence inflammatory responses in various organs by disrupting the oxidant-antioxidant system in the body [22]. Lead can generate reactive oxygen species (ROS) by altering the cellular redox status by directly binding to proteins due to its high electronegativity. Long-term exposure to lead in adults and children results in adverse effects such as difficulties in intellectual and learning ability and behavioral disorders [31]. Mabrouk and Hassen studied the antioxidant system suppression in rat kidneys [32]. Results showed that the rat group exposed to lead showed a significant decrease in enzymes such as glutathione, catalase, glutathione peroxidase, and superoxide dismutase.

2.5 Chromium

Chromium causes several health issues as a result of employing it in industrial applications. Natural causes such as erosion of chromium rocks and volcanic eruptions release chromium into the environment. Chromium has been employed in almost all industries since its identification in 1797 as a crystallized red mineral by Louis Nicolas Vauguelin. It produces almost 10 million tons of products per year all over the world. Worldwide concentrations of chromium in rivers and lakes range between 26 μg/L to 5.2 mg/L, about 5 to 800 μg/L in seawater, and about $1 - 300$ mg/kg in groundwater [33]. In India, the chromium level in the environment exceeds the normal range of 2 mg/L to $2000 - 5000$ mg/L, and $2000 - 3000$ tons of chromium are released from the tannery industries [34]. Cr(VI), an oxidation state of chromium, is known to be a human carcinogen by the WHO, and the intake of chromium mixed water leads to cancer mortality [35]. The genotoxicity mechanism of Chromium (VI) involves its entry into the cell via a sulfate transport system. Once inside, it is converted to its trivalent form through the action of cellular enzymes, including glutathione (GSH), ascorbic acid, cytochrome P-450, glutathione reductase, and riboflavin. Inhalation of Cr (VI) released from chromium-related industries results in irritation of the respiratory tract, airway irritation, and obstruction of the airway, which in turn causes lung, sinus, and nasal cancer [36]. Inhalation exposure of chromium concentration beyond 0.001 mg/m^3 leads to various ulcers and cancers. Inhalation of chromium in pregnant women affects the fetus by placental transfer [37]. For early identification of heavy metal exposure and timely intervention to safeguard public health, it is critical to use accurate sensor-based diagnostic methods to detect even trace amounts of heavy metals.

3. Conventional methods to measure HMs

Traditional detection methods encompass a range of analytical techniques for analyzing heavy metals in samples. Methods like atomic absorption spectroscopy (AAS), inductively

coupled plasma mass spectroscopy (ICP-MS), hydride generation atomic absorption spectroscopy (HG-AAS), and high-performance liquid chromatography (HPLC) hold significant potential despite their respective constraints [4].

3.1 Atomic absorption spectroscopy (AAS)

The AAS technique, which utilizes free atoms in the gaseous phase to absorb light, has been widely used in the past decade. Atomizing a sample and exposing it to a beam of light appropriate for the target metal is a method of determining its composition. The amount of light absorbed in a sample is proportional to its metal concentration. AAS offers excellent sensitivity and selectivity, making it suitable for detecting a wide range of HMs in various matrices [38]. Improvements in Electrothermal Atomic Absorption Spectrometry (ETAAS) have significantly broadened its applicability in trace element analysis. These advancements have led to heightened sensitivity, detection capabilities, and result reproducibility, surpassing previous limitations like matrix interferences and background absorption. New modifiers and trapping techniques stabilize analytes, while precise control over atomization temperature and atomizer design further boost performance [39]. The introduction of high-resolution continuum source ETAAS facilitates directs solid sampling, enabling swift quantitation with minimized background noise. Moreover, ETAAS automation, particularly through flow injection analysis (FIA) and chemical vapor generation, allows for the cost-effective and efficient analysis of elements like as and Hg in environmental samples or in food ingredients, presenting a viable alternative to methods such as Inductively Coupled Plasma Mass Spectrometry (ICP-MS).

3.2 ICP-MS

ICP-MS is an ion source coupled with mass spectrometry for elemental analysis. The sample is introduced into the high-temperature plasma, where it is atomized, ionized, and subsequently analyzed by mass spectrometry. ICP-MS provides exceptional sensitivity and allows simultaneous detection of multiple HMs with high precision, making it a preferred choice for trace metal analysis [40]. ICP-SFMS, or Sector Field ICP-MS, stands out in its ability to detect very low concentrations of elements and compounds with high precision. Its advanced resolution makes it particularly adept at handling complex samples where different species of elements need to be distinguished from one another. This makes it invaluable in various fields, such as environmental analysis, biochemistry, and materials science, where understanding the exact composition of samples is crucial. On the other hand, MC-ICP-MS, or Multicollector ICP-MS, takes precision to another level by allowing scientists to measure isotope ratios with exceptional accuracy [41]. This capability is especially important in fields like geology, archaeology, and nuclear science, where understanding the ratios of different isotopes provides insights into processes such as radioactive decay, geological formation, and even the origins of celestial bodies.

3.3 Hybrid generation atomic absorption spectroscopy (HG-AAS)

HG-AAS is an advanced technique for HM sensing that combines the principles of traditional AAS with a unique sample introduction method. In HG-AAS, volatile compounds of the target HMs are generated in situ by chemical or electrochemical means, such as hydride or cold vapor generation. These volatile species are then transported to the atomization source, typically a flame or graphite furnace, where they undergo atomization and subsequent absorption of light at specific wavelengths. HG-AAS offers enhanced sensitivity and selectivity compared to conventional AAS methods, particularly for trace-level analysis of HMs in complex sample matrices [42].

3.4 High-performance liquid chromatography (HPLC)

HPLC-based HMs sensing, the sample is injected into a chromatographic system equipped with a stationary phase capable of selectively retaining metal ions while allowing other components to elute. Various stationary phases, such as ion exchange or chelating columns, can be employed depending on the specific metal ions of interest. Detection is typically achieved using a suitable detector, such as a UV-Vis or fluorescence detector, capable of quantifying the eluted metal ions based on their characteristic absorption or EMspectra. HPLC offers several advantages for HM sensing, including the ability to separate and quantify multiple metal ions simultaneously, even at trace levels, in complex sample matrices [43].

Most of the detection principles exhibit considerable sensitivity and selectivity for detecting heavy metal ions. These methods work by observing changes in the optical signal or electrical signal resulting from the interaction between the recognition element and the target metals, thereby providing information about the target HM's concentration. However, when used for field testing in various environments (such as wastewater, seawater, and biological samples), pH and water quality differences can lead to inconsistent results, reducing reproducibility. Additionally, existing detection methods often struggle with poor selectivity due to interference from other ions present in the environment. The complexity of microelectrode manufacturing techniques also hinders further development of these detection methods. Despite the efficiency in sensing HMs by all these conventional methods, it possesses some other disadvantages such as sample preparation complexity, limited sensitivity (can detect only up to μg level), interference in detection from matrix components, inability to detect multiple metals at a single time, instrumentation costs and lack of real-time monitoring. Addressing all these disadvantages of conventional methods, researchers have identified that nanomaterial-based sensors could promisingly overcome these limitations and offer detection of HMs in trace levels [44].

4. Role of nanomaterials in sensing

As discussed earlier, the limitations caused by conventional methods need to be addressed to improve the selectivity and sensitivity of HMs detection. The chemical sensors, especially those incorporating nanomaterials, present promis-

ing solutions for on-site detection. Nanomaterial-based sensors capitalize on features like extensive surface area, high catalytic efficiency, and robust adsorption capacity [45–48]. These sensors commonly utilize metallic nanoparticles, carbon-containing nanomaterials, and mesoporous or silicon nanoparticles. Their heightened sensitivity is attributed to their strong reactivity, large surface-to-volume ratio, good adsorption, and properties dependent on size. Techniques such as nanocomposite formation and covalent functionalization further amplify sensitivity and selectivity. The integration of nanomaterials has also improved the detection and reproducibility limits. Moreover, nanotechnology facilitates miniaturization, enabling the development of lab-on-chip technology that makes an easier route to develop on-site detection. The nanomaterials widely used for sensing applications are discussed below.

4.1 Silica nanoparticles

Silica nanoparticles have a high surface area to volume and excellent adsorption ability for HMs, making them attractive materials for HM detection [49, 50]. The mesoporous structure of silica NMs provides a large number of accessible binding sites, facilitating the selective detection of HMs even at trace levels [51]. They can be modified to carry particular ligands or receptors that have a strong affinity for heavy metals, allowing for highly selective detection. [52]. The optical properties of silica NMs can be tailored to develop FL-based sensors [53]. The stability and robustness of silica-based NMs make them suitable for their use in harsh environments, ensuring real-world metal sensing applications [54]. Santhamoorthy et al. developed a chemosensor based on silica nanoparticles by incorporating propidium iodide aimed at sensing various HMs but later found to be specific for Fe^{3+} [55]. A significant color change from pink to orange signified the presence of Fe^{3+} ions in the aqueous media. Stoian et al. fabricated a fluorescent-based sensor for iron, copper, and cobalt sensing [56]. For designing the sensor they employed terbium, a luminescent material, along with silica nanoparticles (TBL@SiO_2). The FL was quenched in the presence of Cu^{2+}, Fe^{3+}, and Co^{2+}, indicating the sensor's sensing ability. The designed luminescent probe displayed a superior response towards transition metal ions than other reported probes. Similarly, Srinivasan and colleagues created a core-shell structure designed for the targeted detection of mercury ions in environmental specimens [57]. The synthesized core-shell silica nanoparticles immobilized DNA and were based on DNA hybridization with mercury ions forming (Thymine-Hg^{2+}-Thymine) base pairs. Cetinkaya et al. fabricated a nano chemosensor for the sequential detection of Pb^{2+} ions [58]. They synthesized silica nanoparticles tagged with fluorescein, where the FL quenching is a result of the complexation between the amide groups on the surface and Pb^{2+} ions. This nanoscale chemical sensor demonstrates a limit of detection (LOD) at a remarkably low level of approximately 850 nm.

4.2 Metal-organic frameworks (MOFs)

MOFs or metal-ligand architecture is a 3D crystalline porous nanomaterial that mainly consists of metal cations linked together by linker ions or organic strut. There are various acceptable combinations of organic linkers available with metal ions and structural motifs, resulting in the formation of new MOFs [59]. Coordination bonds between zinc, nickel, zirconium, or other transition metals result in the formation of the most common MOFs, such as ZIF, MIL, and UiO [60]. MOFs possess numerous advantages, such as being highly porous, having vast surface area, tuneable pore size, and wide opened chelating sites that enable them to be widely used in fields of drug delivery, catalysis, sensors, energy storage, and conversion, gas storage, and separation and metal ions sensing [61]. Nguyen et al. developed a new MOF-based nanomaterial for improving the electrochemical sensing of Cd^{2+} and Pb^{2+} [62]. They utilized Ytterbium, a rare earth metal, as a core linked by benzenetricarboxylic (BTC) ligands for MOF synthesis using the hydrothermal method. The resulting MOFs had a vast surface area of 1162 $m^2\ g^{-1}$. The synthesized MOFs showed an LOD of 3.0 ppb for Cd^{2+} and 1.6 ppb for Pb^{2+}. Hossain et al. developed a recyclable nanocomposite using MOF and polymer thin film for fluorometric detection of Hg^{2+} and ranitidine [63]. They developed a thiourea-functionalized aluminum-based metal-organic framework. These MOFs showed a LOD of 7.3 nM and 3.4 nM for Hg^{2+} and ranitidine, respectively. Ansari et al. developed nickel-doped MOFs for fluorometric detection of Hg^{2+} and Fe^{3+} [64]. The synthesized MOF exhibited the "On" and "Off" FL mechanisms. The MOFs showed "Turn-off" for Hg^{2+} and Fe^{3+} and "Turn-on" for Cr^{4+} and Al^{3+}. This sensor showed the lowest LOD of 7.98×10^{-7} M for Hg^{2+}.

4.3 Magnetic nanoparticles

Magnetic nanoparticles have gained attention as potential materials for HM sensing, attributed to their unique characteristics, including a vast surface area, superior magnetic response, and easy surface modification capabilities [65, 66]. These nanoparticles offer multiple benefits for sensing applications, including improved sensitivity, quicker detection times, and the convenience of being easily separated from the sample matrix through the application of an external magnetic field. Functionalization of magnetic nanoparticles with specific ligands enables selective recognition and binding of heavy metal ions, allowing for precise detection and quantification. Fe_3O_4 is the most employed magnetic nanoparticle, which belongs to the class of metal oxides [60–67]. Zargoosh et al. developed a nano adsorbent to effectively detect and remove heavy metal ions from industrial wastewater [68]. The prepared nano adsorbent covalently immobilized the thiosalicylhydrazide on the surface of magnetic nanoparticles (Fe_3O_4). This nano adsorbent showed different adsorption capacities for metals, such as 188.7, 107.5, 76.9, and 1.3 mg/g for Pb^{2+}, Cd^{2+}, Cu^{2+}, and Zn^{2+}. Using the Hydrothermal method provided hydrophilic proanthocyanidins-functionalized Fe_3O_4 nanoparticles. A novel magnetic nanoparticles sensor was developed by immobilizing BODIPY compound APTMS functionalized silicon-coated magnetic nanoparticles (APTMS-SiO_2@Fe_3O_4) and was named F-SPION [69]. The F-SPION underwent trials with different metal ions, yet it demonstrated a 'turn-off' fluorescence exclusively for Cr

(VI), accompanied by a noticeable shift in color from brown to yellow. Selectivity experiments conducted on F-SPIONS combined with Cr (VI) in the presence of various metal ions revealed consistent intensity levels before and after introducing Cr (VI). However, there was a marked reduction in intensity, specifically when Cr (VI) was present. Investigations into the pH responsiveness of F-SPIONS in combination with Cr (VI) across a range from pH 1 to 8 determined that a pH of 1 is ideal for detecting Cr (VI), with a limit of detection (LOD) at 0.0033 grams per liter.

5. Carbon dots

CDs are intriguing due to their unique characteristics, which include wavelength-dependent emission of colors, excellent water solubility, low toxicity, and higher biocompatibility [70–72]. These properties make CDs a versatile option as semiconductor nanomaterials for the accurate detection of HMs in environmental samples, given their strong fluorescence [73, 74]. Additionally, their environmentally friendly nature has highlighted their potential for applications in environmental remediation [75–77]. The interaction between these probes and HMs leads to alterations in the spectroscopic nature of the fluorophores, such as FL intensity, lifetime, and wavelength [78]. Compared to conventional fluorescent sensor molecules, CDs are more resistant towards photobleaching. The semiconductor quantum dots are equally effective as CDs [79]. However, several issues limit its uses in biological and environmental applications, including the toxicity profile and intrinsic blinking. Concerning the metal content of quantum dots, they are restricted from being used for environmental applications. The intrinsic blinking characteristic of quantum dots doesn't allow the long-term monitoring of a single molecule. Furthermore, due to the easier surface modification process, the quantum yields (QY), selective binding, and solubility can be improved [80, 81].

5.1 Optical properties

CDs exhibit a range of unique and promising optical properties, which remain consistent even when synthesized from various precursors and through different processes. These properties include strong photoluminescence, which is highly dependent on the excitation wavelength, allowing for tunable emission colors. Additionally, CDs demonstrate excellent photostability and high quantum yields, making them suitable for a variety of applications. The following section provides a detailed discussion of the optical properties of carbon dots.

5.1.1 Absorbance

CDs display significant absorbance in the ultraviolet (UV) spectrum, with primary peaks typically occurring between 250 and 320 nm. Additionally, they often have a secondary, less intense absorbance peak extending into the visible light spectrum. During their synthesis, CDs can exhibit various UV absorption peaks depending on the specific conditions and methods used. Furthermore, altering the surface chemistry of CDs can lead to slight shifts in their absorption wavelengths and enhancements in their absorption peaks, thereby fine-tuning their optical properties and making them more versatile for different applications [82]. The characteristic absorption peaks of CDs are ascribed to the $\pi - \pi^*$ transitions within the conjugated C=C structures and the $n - \pi^*$ transitions associated with C=O, C-N, or C-S functional groups. [83]. Jiang et al. described the synthesis technique for creating multimode-emissive carbon dots, utilizing phenylenediamine (PD) and polyvinyl alcohol (PVA) [84]. The ethanol-based solution of the multimode emissive carbon dots displayed two prominent absorption peaks at 247 and 355 nm, which correspond to the $\pi - \pi^*$ transition and the $n - \pi^*$ transition, respectively. Yiye and their team employed both L-cystine and D-cystine to produce carbon dots characterized by high FL [85]. The carbon dots derived from L-Cystine exhibited two separate absorption peaks within the spectrum: one at 243 n resulting from the $n - \pi^*$ transition, and another at 300 nm due to the $\pi - \pi^*$ transition. Upon absorbing light within the ultraviolet or visible range, these carbon dots experience fluorescence with a Stokes shift spanning several tens of nm.

5.1.2 Photoluminescence (PL)

CDs exhibit a highly intriguing feature known as photoluminescence (PL). However, the full mechanism behind this phenomenon has not been thoroughly elucidated by researchers and remains a topic of debate. It is still uncertain whether this distinct property is attributed to the varying sizes of the nanoparticles and the functional groups on their surfaces or if it arises from an entirely different mechanism [86, 87]. Wang et al. synthesized highly luminescent amorphous CDs using organosilane as a coordinating solvent [88]. The prepared CDs had a QY of 47% and were 1.54 nm in size. When this CD was excited at 380, 460, and 540 nm, it showed a Stoke shift at 460, 540, and 620 nm, respectively. The emission spectra of the synthesized CDs depend on the excitation wavelength. Theoretical calculations first proposed the relationship between PL and CDs. Liu and the team suggested that the quantum size effect is predominantly responsible for photoluminescence, while the defect state has a lesser impact [89]. Yu and colleagues have stated that both the carbon core and surface states play essential roles in the energy transfer process [90]. They synthesized six different CDs, 3 with rich carbon sources using glycine (CD_1), alanine (CD_2), and valine (CD_3) and 3 with rich nitrogen sources using leucine (CD_4), histidine (CD_5), and CD_6 from arginine. They investigated the effects of carbon core on the PL property of CDs using emission spectra of CD_{1-6}. The emission spectra of carbon dots labeled CDs_{1-3} revealed emission at 445 nm and 305 nm, with the intensity of the 305 nm peak intensifying as the carbon content increased. Similarly, the excitation peaks for carbon dots CDs_{4-6} were observed at 250 nm, 275 nm, 325 nm, and 365 nm. However, the peaks at 250 nm and 365 nm progressively diminished with the rise in nitrogen content and vanished entirely for CD_6. This suggests that the carbon core and nitrogen content are significant factors influencing the photoluminescence properties of CDs. To prove the surface state effects of PL property, CD_6 was

taken for its abundant nitrogen content and treated in pH $1-14$; the alkalinity of the solution doesn't affect the EM peak of CD_6 centered at 445 nm where in acidic conditions amino groups on the surface state of CD_6 gets affected and results in the appearance of new EM peaks at 410 and 500 nm, concluding that surface states also contribute towards PL property. Moreover, the synthesized CDs exhibited sensitivity to the concentration of Fe^{3+} within an LR of 12 to 250 μM and with a size of $2-4$ nm. Fang et al. came up with the idea that the CDs' PL property arises due to the interaction between isolated derivatives of pyridine molecules and defect states in the CD's surface [91]. The PL EM of the CDs originates from a composition featuring isolated sp2 clusters, interconnected pyridine derivative units, plentiful defect states, and graphitic cores.

5.1.2.1 Fluorescence (FL)

CDs are employed in sensing applications because of their well-explored tuneable FL property. A Jablonski energy diagram is shown in Figure 2 to demonstrate the fluorescence emission properties. FL in CDs is because of three major origins: a) core-state EM as a result of perfect carbon core and less surface passivation, b) surface-state EM due to the surface-modified groups, and c) molecular FL arising due to by-products during the preparation of CDs. The emission linked to the surface state might correlate with the level of oxidation on the surface and the types of functional groups that are present. Reports to date regarding the FL of CDs have arisen mainly due to the degree of surface oxidation state. The surface defect state in CDs is directly proportional to the degree of surface oxidation, which in turn can capture excitons. Radiations from these excitons cause red-shift EM of CDs. Different energy levels on the CDs can be developed by immobilizing various functions on the surface of the CDs. The quantum confinement effect is a key characteristic of CDs that influences FL EM. This effect causes a significant change in electron distribution within the nanometer-scale semiconductor crystals, leading to the display of properties like a bandgap and size-dependent energy relaxation dynamics [92]. QCE of CDs occurs when the quantum dot size is lesser than the exciton Bohr radius [93]. Jiang et al. reported the synthesis of three different types, which, under a single ultraviolet excitation wavelength, emit three different FL emissions: red, green, and blue [94]. Hence it was concluded that the quantum confinement effect plays a major role in the FL emission. Liu et al. reported the fabrication route of CDs using the microwave method using molecular precursors of o-phenylenediamine, p-phenylenediamine, and n-phenylenediamine show wavelength-independent excitation, with a QY value of 4.5, 7.5, and 14.3% respectively [95]. The degree of FL EM with various colors depends on the surface functional groups of the CDs. Yuan et al. fabricated green-CDs5 and red-CDs5 with QY values of 81% and 85% using perylene as the starting material [96]. Nitrogen doping on CDs has a different impact and is the widely studied potential doping system in CDs; the EM properties of N-doped CDs have a red shift of EM wavelength and an increase in FL QY. Concentration in CDs is majorly responsible for the EM wavelength color [97]. Chen et al. reported the synthesis of concentration-dependent CDs69 from Citric acid and ethanolamine with an EM wavelength range from 514 nm to 585 nm using the hydrothermal method [98]. Chinese ink was oxidized to obtain the precursor molecule CDs and doped with heteroatoms N & S for sensitive detection of Cu^{2+} and Hg^{2+} [99]. They proved that heteroatoms play an important role in tunable PL properties by confirming via PL EM and PL excitation (PLE) spectra of CDs. The doped CDs had a size of $1-6$ nm and a good QY.

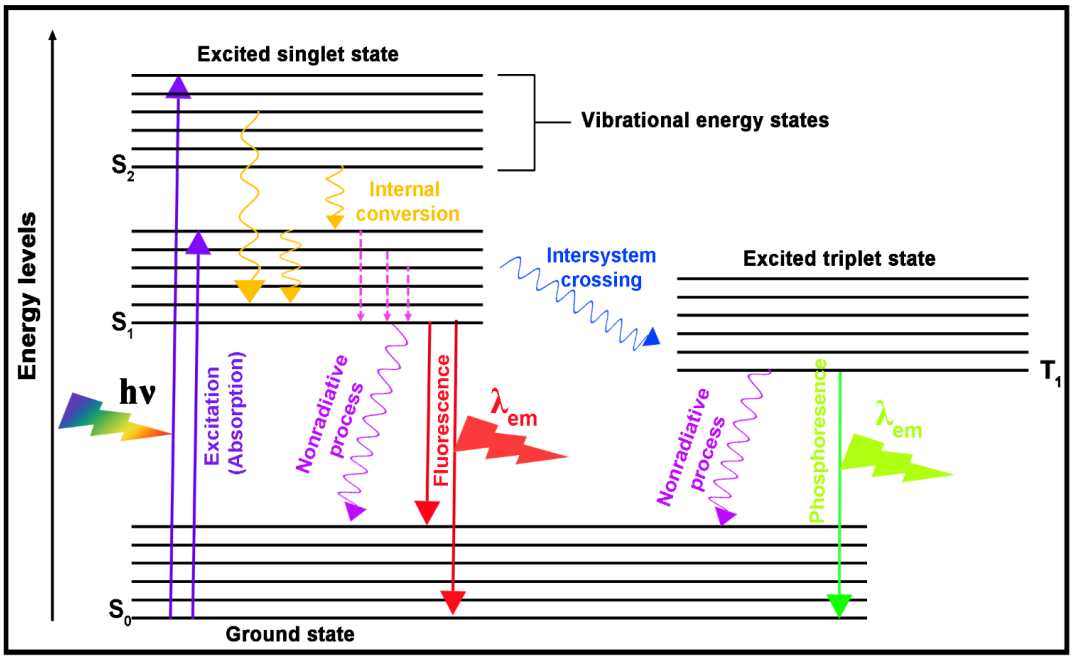

Figure 2. Schematic representation of absorbance, fluorescence and phosphorescence.

5.1.2.2 Phosphorescence

CDs are most studied for their properties of FL, but recent studies have also focused on the study of CDs for their properties of phosphorescence [100]. In 1974, Paynter's group introduced a new method of detection using room-temperature phosphorescence known as RTP photometry [101]. Once after absorbing the ultraviolet and visible light, the electrons excite from the singlet ground state (S0) and reach the excited state (S1), and as a result of the intersystem crossing process (ISC), the electrons in the S1 state reach the triplet state (T1). The transition of electrons from the ground state to the different excited states by absorbing ultraviolet and visible light reaches the ground state by emitting phosphorescence (Figure 2). Phosphorescence has a variety of superior applications when compared to FL. It exhibits a large EM period, a comparatively larger stokes' shift, and is sensitive to environmental characteristics [102]. Li et al. proposed a well-established procedure to aid phosphorescence by using water molecules to introduce intermolecular hydrogen bonds between cyanuric acid and polymer-coated CDs [103]. They proved that the phosphorescence of CD-CA powder could increased by the addition of water molecules. The phosphorescence property of CD-CA powder is three times comparatively increased CD-CA in water, with an increase in phosphorescence lifetime of 0.253s to 0.687s. Tian et al. used varying annealing temperatures to treat the CD@PVA and observed that after 200 °C, phosphorescence EM had started [104]. Therefore, this implies that the annealing temperature influences the phosphorescence emission. Li et al. proposed a method of synthesizing fluorescent CDs that includes both oxygen and nitrogen atoms using folic acid as raw material via hydrothermal method [105]. Then, it was incorporated into a composite matrix to obtain NCDs, resulting in a phosphorescence QY of up to 7%. Wang et al. established a method for preparing RTP CDs by molten salt method, which involves the use of organic salt to calcinate triaminobenzene [106]. These synthesized CD composites exhibited well-observable RTP properties and a QY of 26.4%. This method can be employed for almost all carbon precursors, and adjusting the mass ratio of reaction temperature, amount of carbon precursor, and time results in better RTP performance.

5.2 Physical properties

5.2.1 Surface passivation

Surface passivation plays a crucial role in shielding the surface of CDs from contact with organic substances, thus maintaining their optoelectronic characteristics. Treating the surface of carbon dots with polymeric PEG1500 via acid treatment not only boosts their fluorescence but also aids in their functionalization [107]. Moreover, the FL modulation of CDs can be achieved through treatments with different molecular weight branched polyethyleneimine (b-PEI), polyethylene glycol (PEG), and diamine-terminated oligomeric PEG, resulting in the formation of polyamine-passivated CDs and CDs treated with free amines [108]. Burlinos et al. utilized a pyrolysis technique involving citric acid and amine groups to fabricate surface-passivated CDs, where citrate acted as the carbon core and amines functioned as surface functional groups [109].

5.2.2 Doping

Doping the CDs with heteroatoms is a major route to tune the intrinsic structure of CDs. Incorporating heteroatoms into CDs alters the surface functional groups and electron distribution. This change affects the band gap between the highest occupied molecular orbital (HOMO) and the lowest unoccupied molecular orbital (LUMO), which in turn, modifies their fluorescence characteristics (Figure 3). Adjusting the quantity and type of heteroatom can enhance or diminish the FL efficiency of CDs, as well as modulate their EM peaks. To significantly improve the QY of CDs, non-metallic dopants such as nitrogen or silicon can be incorporated into the CDs to modify their band structure. Additionally, metallic dopants play a role in limiting the overabundance of amino and carboxyl groups in the precursor molecule, such as citric acid, during dehydration and carbonization. This is achieved through the chelation process between metal ions and chemical groups [110, 111]. The nitrogen doping of carbon dots (CDs) surfaces can markedly enhance their emissive properties. Following nitrogen doping, CDs transition from exhibiting multiple transition modes to a single transition mode, where EM exclusively arises from radiative transitions of sp^2 carbon. This phenomenon leads to excitation-independent FL. This also results in dense electron cloud activity and a red-shift in the absorption peak, resulting in a narrow energy gap. The most common sulfur sources are sodium sulfide, thiomalic acid, sodium thiosulfate, heparin sodium, and cysteamine hydrochloride. Doping carbon dots (CDs) with sulfur enhances their electronic structure by improving the density of states or creating emissive trap states for photoexcited electrons. This process also leads to modifications in the band-gap energy of the CDs [112]. Doping phosphorus can subsequently increase the luminescence efficiency of CDs. Phosphorus with the carbon cluster forms substitutional defects and acts as n-type donors, therefore modifying the electronic and optical properties [113]. Zhang's research team developed tellurium-doped carbon dots (Te-CDs) utilizing a carbon source derived from Te-containing molecular probes [114]. These Te-CDs exhibit a remarkable capability for the sensitive detection of superoxide anions. The reversible detection ability of superoxide anions is based on the redox properties of Te-centres present on the surface of Te-CDs, enabling detection with high sensitivity and a low detection level of up to 8.0 pm. Furthermore, the introduction of metallic copper doping into carbon dots (Cu-CDs) significantly broadens and enhances the absorption band compared to undoped CDs, indicating strong optical trapping capabilities. Commonly used copper sources for doping include acetate monohydrate, cupric nitrate, and cuprous chloride. Du et al. developed gadolinium-doped CDs and used them as T_1 contrast agents for FL and magnetic resonance dual-modal imaging, which also exhibited lower toxicity and improved stability [115]. The QY of gadolinium-doped CDs was around 48.2%.

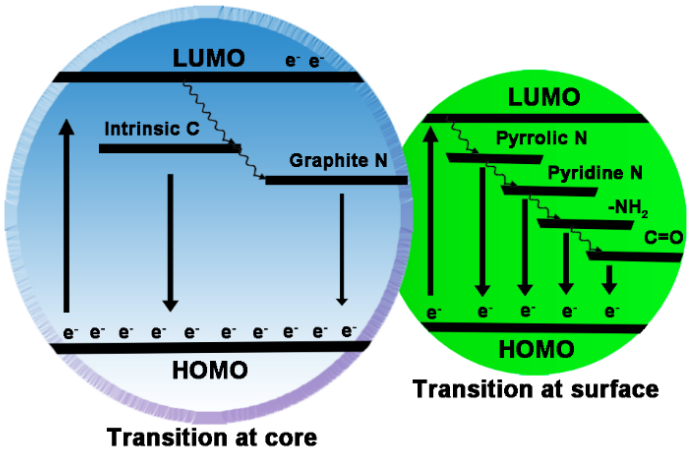

Figure 3. Emission mechanism involved in carbon dots where surface chemistry plays a major role.

5.2.3 Photostability

The photostability property is that fluorescent materials should not lose their energy when continuously exposed to UV or visible radiation. CDs' photostability is contributed by their large π-conjugated structural framework. Photostability is those CDs that show fixed EM wavelengths under varied excitation wavelengths. Jiang *et al*. fabricated CDs from indocyanine green (ICG-CDs) via the hydrothermal method, which exhibited stability under various temperatures and anti-photobleaching properties when compared to traditional IGC [116]. It also exhibited stability under all pH conditions with enhanced photothermal conversion efficiency. These ICGCDs served well as contrast agents in NIR bioimaging and photothermal agents. Zhi *et al*. developed four types of CDs with citric acid and malic acid doped with phosphorous (CACDs, CA- P-CDs, MACDs, MA- P-CDs). Photostability studies revealed that 40 minutes of exposure to CA-P-CDs-4 had higher photostability than CA-CDs, and 60 minutes of exposure to MA-P-CDs-4 approximately 25% higher than MA-P-CDs proved that phosphorus doping improves the photostability of CDs.

5.2.4 Sensitivity

CDs with functional groups such as -OH, -NH_2, and -COOH on their surface exhibit high sensitivity to metal ions. The PL EM of CDs is highly sensitive to HMs because of the interaction between surface functional groups and metal ions, which results in strapping bonds or faster coordination between them [117]. The sensitivity of CDs is very important in detection. Hence, CDs are functionalized with appropriate surface ligands that are very specific to the target analyte. This can be done by two methods: the non-enzymatic approach and the enzymatic approach. Radhakrishnan et al. synthesized a nanocomposite using green CDs from butter juice and graphitic carbon-nitride (C_3N_4) nanosheets [118]. The prepared CD@C_3N_4 was tested for its detection ability of Cr (V), Cu (II), and Pb (II) in real water samples. The prepared composites showed high selectivity towards Cr (V) due to the surface functional groups of prepared nanocomposites. Cu(V) and Pb(II) showed strong access to surface functional groups of prepared nanocomposites. These prepared nanocomposites had a LOD of 0.54, 0.18, and 0.2 nm for chromium, copper, and lead [118]. Another non-enzymatic approach is passivating aptamers on the surface. Zhao et al. developed a novel aptasensor for the detection of cadmium [119]. A one-step dehydration method was utilized to synthesize CDs using citric acid and ethylenediamine as precursors and to functionalize them with CD4 aptamer. The complex NCDs-CD4 aptamer binds to the target molecule cadmium via electrostatic interaction, with a LOD value of 0.89 μg/L and LOQ value of 2.68 μg/L. The value obtained from this aptasensor was matched with the ICP-MS method, which showed similar accuracy and superiority.

5.3 CDs Mechanism of metal sensing

CDs are widely used in the field of sensing owing to their unique optical properties. The CDs interact with metal ions either by colorimetric or FL methods. The colorimetric method is a visible change in solution due to the interaction of CDs and metal ions. FL detection of heavy metal ions is carried out by observing the change in the EM of the CDs. Quenching mechanisms (Figure 4) occur due to energy transfer between CDs and Heavy metal ions. The major mechanisms of HMs detection by CDs are explained below:

5.3.1 Fluorescence quenching

The most extensively debated method of HM sensing by CDs involves Fl quenching. When certain metal ions coexist with carbon dots in a solution, they can cause fluorescence quenching. This quenching can happen through mechanisms such as energy transfer, charge transfer, or the formation of non-fluorescent complexes. The decrease in fluorescence intensity or emission is due to the metal ions absorbing energy or electrons from the excited carbon dots. The effectiveness of quenching is primarily influenced by the concentration of metal ions and the affinity of the CDs for this ion [120].

5.3.1.1. Metal-enhanced fluorescence (MEF)

MEF is similar to FL quenching but shows an increase in

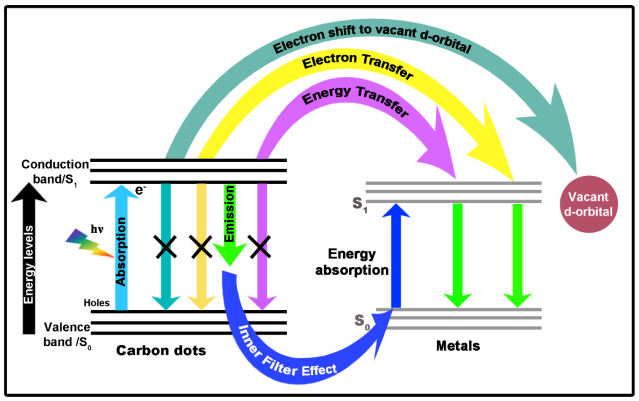

Figure 4. The possible mechanism of heavy metal sensing using carbon dots, where electron transfer, energy transfer, and the inner filter effect play a major role in quenching the fluorescence of CDs in the presence of heavy metals.

the EM intensity of CDs due to the presence of metal ions [120]. Metal-enhanced FL occurs due to an increase in resonance energy transfer between the excited CDs and free surface HMs [121]. The presence of metal ions can induce localized surface plasmon resonance effects, thereby generating an augmented electromagnetic field around the CDs. This intensified electromagnetic field boosts the radiative decay rate of the CDs, leading to enhanced FL EM [122].

Apart from these two major mechanisms of HMs sensing by CDs, chemists also proposed another major mechanism in sensing of HMs by CDs such as complex formation, inner filter effect (IFE), photon-induced electron transfer (PET), and aggregation-induced EM enhancement (AIEE).

I. Complex formation mechanism

The complex formation mechanism includes the surface functionalization of CDs, which causes chelation or coordination of HMs. Typically, the surface of the CDs contains oxygen-containing groups such as -OH, -COOH, -OR, C=O, etc. In addition, the CDs are doped with sulfur, nitrogen, and other dopant groups containing -NO_2, -NH_2, -SOH, -SH, and -CN groups. This group donates a lone pair of electrons to the metal ions resulting in a coordination complex formation [123]. Bandi et al. described the possible quenching mechanism of NCDs. He stated that the complex formation may arise due to a simple increase in the absorption supporting UV-spectrum data [124].

II. Inner filter effect (IFE)

IFE is a non-radiative energy mechanism. This occurs due to the absorption of excited or emitted radiation by the CDs [123]. IFE is a non-irradiative energy conversion phenomenon where absorbers in a detection system absorb excitation and/or emission radiation from fluorophores. Effective IFE requires the absorbers' absorption spectra to overlap with the fluorophore's excitation or emission bands. This process transforms analytical absorption signals into fluorescence signals. The primary inner filter effect refers to the absorption of excitation light by absorbers, while the secondary inner filter effect pertains to the absorption of emitted light. Due to the lack of chemical covalent interactions between absorbers and fluorophores, IFE is straightforward, easy to implement, and cost-effective. This mechanism can take place in two ways-as one of the quenching spectrums overlaps with the excitation spectrum of CDs, the quenching process is triggered by light absorption by the quencher and the CDs are quenched as a result [125]. The other mechanism involves reabsorption in the quenching process, and photons are emitted by one species and absorbed by another, which occurs because unused quenchers and CDs weaken the absorption or excitation radiation in the solution [126].

III. Photon-induced electron transfer (PET)

This mechanism makes fluorometric sensing of metal ions by various CDs take place. In the PET mechanism, a metal ion accepts an electron from the CDs in the excited state, forming a complex and returning to the ground state without releasing any photons [127]. PET mechanisms of CDs contain two major molecules: oxidative and reductive pet. A carbon dot-based sensor was developed for effective sensing of picric acid [128]. A Cyclic Voltogram was utilized to prove the effective quenching mechanism between picric acid (PA) and CDs.

−0.56 V was calculated as the onset reduction potential of CDs with a bandgap value of 3.29 eV. The HOMO and LUMO values of PA were comparatively lesser than the HOMO and LUMO values of CD. This indicates that a possible charge transfer may occur from CD to PA.

IV. Aggregation-induced EM enhancement (AIEE)

Aggregation of CDs has been induced by temperature, solvent, and additives like HMs results in the AIEE mechanism. This blocks the intramolecular CD movement and results in the blocking of non-radiative path and activated radioactive decay [129]. Zhang et al. hydrothermally synthesized orange-yellow CDs for the detection of Cu^{2+} ions [130]. The O-CDs form a complex with Cu^{2+} and result in an aggregation-induced emission enhancement mechanism with an LR of 0.02 to 30 μm with an LOD of 14 nm.

5.4 Types of detection method

5.4.1 Optical sensors

Optical sensors for the sensitive detection of HMs overcome the expensive and laborious processes of sample preparation possessed by standard laboratory-based techniques such as AAS, XPS, ICP-AES, and ICP-MS [131]. Optical chemical sensors (OCS) rely on the immobilized indicator (organic dye) to change its optical properties, such as absorption, emission, transmission, and lifetime, upon interacting with the analyte. OCS utilizes electromagnetic radiation, which, when interacting with the sample, alters the optical characteristics of the indicator. These changes can then be correlated with the concentration of HMs [132]. OCS based on mesoporous materials is generally based upon light absorption or light emission. The OCS of the analyte concentration is measured based on the change in the optical properties of the indicator after being illuminated by electromagnetic radiation. The sensitivity of EM methods, when compared to absorption-based methods, is 1000 times greater and also has as low LOD as possible towards the anticipated analyte [133]. Even though luminescence intensity-based methods are generally affected by light source intensity, inner filter effects, sample turbidity, and sensing layer thickness, carbon-based OCS offers more advantages than mesoporous materials-based OCS, such as stability, biocompatibility, and lower toxicity [134]. In particular, graphene oxide, a carbon material, exhibits tuneable FL properties based on tuneable size and surface passivation. In general, oxygen groups in GO molecules contribute to a unique pl pattern by opening their band-gap [95, 135]. Green CDs from precursor plumeria plant leaves and fluorescent sensors were developed based on the green CDs for the detection of mercury (Hg^{2+}) and arsenic (As^{3+}) in water and mouse fibroblast cell lines [136]. The developed sensor quenches with Hg^{2+} ions and enhances its EM with As^{3+} ions. The LODs of the developed sensor were found to be around 0.99 nM for Hg^{2+} and 12.15 nM for As^{3+}. Similarly, Yuan et al. developed an aerogel using CDs and cellulose fibrils, which acts as an optical sensor for sensing and adsorbing [137]. The LOD of the sensor was 17.6 mg/L, and the adsorption capacity was 433.5 mg/g.

5.4.2 Colorimetric sensors

Colorimetric sensors have garnered considerable interest owing to their ease of use, affordability, and remarkable sensitivity. They work based on the principle of a color change in response to a specific target analyte. This color change is usually caused by the selective binding of a receptor to the target analyte, leading to a structural change in the receptor and a subsequent color change. There are various materials-based colorimetric sensors, such as nanomaterial-based, smartphone-based, and paper-based sensors, for the sensitive detection of a desired analyte in the sample. Here, we discuss how carbon dots play a major role in the colorimetric sensing of heavy metal ions in the environment. CDs have emerged as promising nanomaterials for colorimetric sensing applications due to their unique optical properties and excellent biocompatibility. In colorimetric sensing schemes utilizing CDs, interactions with analytes, such as heavy metal ions, lead to distinct changes in the optical properties of CDs, including FL quenching or enhancement, aggregation-induced color changes, or pH variations, which can be visually detected without the need for complex instrumentation. These changes are often attributed to mechanisms such as charge transfer, energy transfer, or surface modification induced by the presence of analytes. The specific design of CD-based sensing platforms can be tailored to exploit these mechanisms for selective and sensitive detection of target analytes [138]. Aygun et al. developed CDs doped with heteroatoms like boron, nitrogen, and sulfur for colorimetric sensing [139]. Results showed that doped and undoped carbon dots exhibited detection ability towards metal ions. Undoped CDs detected Fe^{3+} ions (0.187 μM), B-CDs and S-CDs detected Fe^{3+} (0.224 μM) and Ag^{+} 0.174 μM while N-CDs detected Ca^{2+} (0.391 μM) metal ions. Linearity was calculated with the range of 0.06–1.23 μM. With a significant colour change of S-CDs from black to dark brown colour, light brown to grey colour for B-CDs. Bisauriya et al. developed a colorimetric sensor based on CDs doped with nitrogen and sulfur [140]. The sensor detects heavy metals through the absorption-based colorimetric mechanism. This sensor shows a linear increase in the absorption in the presence of Cu^{2+} ions through a complex formation mechanism between the Cu^{2+} and amino groups doped CDs. The other detection mechanism of this co-doped CD, where its pH increased to 9.5 shows an increased response to Cu^{2+} by decreasing the interference effect, with a LOD of 200 nM and linearity of $1-100$ μM.

5.4.3 Electrochemical sensors

Electrochemical sensors employ signal amplification systems such as electrochemical impedance spectroscopy, conductometry, voltammetry, and potentiometry. Electrochemical sensors are rapidly developing to detect HMs. Electrochemical sensors offer various advantages, such as low LOD, high sensitivity, high surface area, good reproducibility, selective detection of more than one metal ion, and a better signal-to-noise ratio [141]. EC sensor's mechanism of action is that potential difference is generated by the output-transducer signal and measured using a potentiostat. Nanoparticles in electrodes of EC sensors offer various advantages such as increased electron and mass transfer rate and Vast surface area. The nanoparticles should possess high reaction activity, a large surface-to-volume ratio, high conductivity, and strong absorption ability. Xiao et al. developed an electrochemical sensor boron-doped diamond electrode for detecting zinc ions using anodic stripping voltammetry. The LOD was calculated at around 2.1 μg/L [142]. These detection methods are shown as proof of concept for sensing HMs in water, even though sometimes it requires sample preparation before subjecting it to treatment. Hence, incorporating CDs in these methods would pave the way for major development in this detection method. The mechanism of CDs-based electrochemical sensing of heavy metal ions involves several key processes, often dependent on the specific interaction between the CDs and the target analyte. Surface functional groups on CDs, such as car-

boxyl, hydroxyl, and amino groups, facilitate the adsorption or complexation of heavy metal ions onto the CD surface. This interaction can induce changes in the electrochemical properties of CDs, leading to alterations in their conductivity or electrochemical response. The presence of heavy metal ions can modulate the charge transfer processes at the CD-electrode interface. This can lead to changes in the electron transfer kinetics or electrochemical reactions occurring on the CD surface, resulting in measurable shifts in the electrochemical signals. Thirdly, the specific functionalization or doping of CDs can enhance their selectivity towards certain heavy metal ions, enabling the development of tailored sensors with improved sensitivity and specificity. For example, nitrogen or sulfur doping of CDs has been shown to enhance their affinity towards metal ions like mercury or lead, respectively [143].

5.4.4 Ratiometric fluorescent sensors

Ratiometric fluorescent sensing is the advanced version of conventional fluorescent sensing and colorimetric sensing. Fluorescent sensing generally gives out enhanced or decreased intensity when in contact with heavy metals. The resultant EM intensity may be interfered with due to unavoidable external factors such as the sample matrix, environmental alterations, and changes in concentration. To reduce this change, another fluorescent material is introduced to produce two EM intensities to evaluate the accurate amount of target analyte in the environment [144]. Ratiometric fluorescent sensors account for measuring two different wavelengths with different intensities without changes hindered by environmental factors (Figure 5). In simple, ratiometric fluorescent probes read out the accurate quantity of heavy metal with two EM intensities when compared to traditional fluorescent sensing with a single EM wavelength [145]. Ratiometric fluorescent sensors also offer a clear visual color change in contact with the heavy metal solution when compared to traditional colorimetric sensing with a particular EM intensity.

Liu and his co-workers worked on a ratiometric fluorescent sensor based on CDs and gold nanoclusters to detect Hg^{+} ions [146]. Lysine-based CDs were synthesized via hydrothermal method and gold nanoclusters using chicken egg white as a reducing agent. The ratiometric fluorescent probe exhibited two EM peaks at 450 nm and 655 nm when exciting under 390 nm with pink FL under UV light. The pH of the solution was adjusted to 7.4 to obtain maximum EM intensity with an optimal reaction time of 7 minutes. The fluorescent probe exhibited changes in the intensity of the 655 nm EM peak when the concentration of Hg^{+} was increased and no changes in the 450 nm peak with linearity in the range of $1-90\ \mu$m for PL intensity ratio of (I450/I655) with a limit of detection of 63 nm. Molecules capable of exhibiting two EMpeaks are widely used for ratiometric fluorescent sensing. Dual fluorescing CDs with EMpeaks centered at $430-500$ nm and $620-700$ nm were utilized for ratiometric sensing of heavy metal ions such as Co^{2+}, Fe^{3+}, Hg^{2+}, and Pb^{2+} [147]. CDs were synthesized via a one-step microwave-assisted method using glutathione

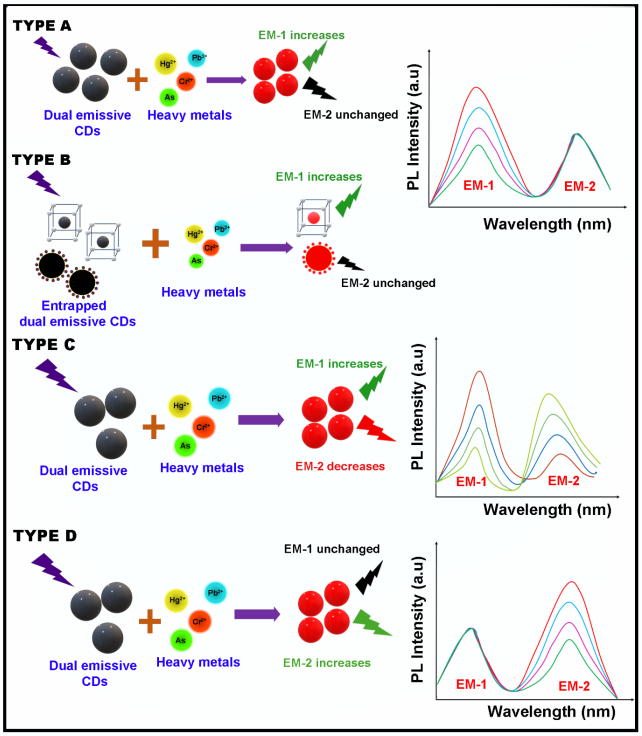

Figure 5. Engineered ratiometric fluorescent carbon dots in the presence of heavy metals – type A: The emission intensity of dual emissive CDs increases at EM-1, whereas EM-2 remains unchanged. Type-B: The emission intensity of dual emissive hybridized or entrapped CDs increases at EM-1, whereas EM-2 remains unchanged. Type-C: Emission intensity increases at EM-1 and decreases at EM-2 when HMs are added to CDs. Type-D: Emission intensity remained the same at EM-1 and increased at EM-2 when HMs were added to CDs.

and formamide. CDs form CD-Pb^{2+} and CD-Hg^{2+} complexes with two distinct EMpeaks centered at 475 and 450 nm. The FL quenching assays were carried out in the range ($1-961$ nm) with CD and metals ions (Co^{2+}, Fe^{3+}, Hg^{2+}, and Pb^{2+}), which showed a LOD value of 96.8, 61.7, 39.5, 37.1 nm. All the assays were carried out in pH close to that of deionized water with no changes in the fluorescent profiles from $4-8$ nm. Förster resonance energy transfer (FRET) mechanism between positive charged amino-carbon dots and negative charged gold nanoclusters was utilized for the ratiometric detection of Pb^{2+} and Cu^{2+} [148]. The CDs were prepared using a microwave-assisted method with arginine and ethylene diamine molecules as precursors. The fluorescent probe CDs/AuNCs were prepared by simple mixing that exhibited two EMpeaks centered at 440 nm for N-CDs and 565 nm for AuNCs. The FRET mechanism of the fluorescent probe CDs/AuNCs was confirmed by the zeta potentials of N-CDs $+17.7 \pm 1.03$ mV and for AuNCs is -6.4 ± 1.4 mV, the fluorescent probe had a value of -3.05 ± 1.1 mV, because of the opposite charge interaction between the N-CDs and AuNCs. The addition of Pb^{2+} to the fluorescent probe (N-CDs/AuNCs) showed that it interacted with AuNCs, resulting in aggregation-induced emission enhancement by inducing the aggregation of Au(I)-thiolate of AuNCs (Au(o)@Au(I)-thiolate core-shell structure). The EM intensity of AuNCs decreased with little changes in the EM intensity of N-CDs, with a visible color change from pink to a strong orange-red color between $2-60$ μm with an LOD of 0.5 μm. The paramagnetic transition of Cu^{2+} ions quenches the intensity of AuNCs with no changes in the intensity of N-CDs by effective charge transfer between Au to Cu^{2+}, resulting in FL quenching of AuNCs in the range of $1-60$ μm with an LOD of 0.15 μm. Thus, the following table explores various types of CDs for ratiometric HM sensing. Ratiometric-based FL sensors based on CDs are also developed with two response EMpeaks in the presence of analytes (HMs). To develop materials with two EMpeaks for ratiometric sensing fluorescent material coated or embedded or hybridized with nonfluorescent materials for dual response signal in the presence of HMs. O-phenylenediamine precursor-based CDs(d-CDs) were synthesized by microwave-assisted method with dual EMpeaks centered at 360 and 530 nm and utilized for sensing Cu^{2+} ions [149]. The prepared d-CDs were tested against increasing concentrations of Cu^{2+} ions (0.8–55 μm), with an increase in peak at 530 nm and quenching of EM peak at 360 nm. The change is the EMpeaks are more specific Cu^{2+} ions than any other metal ions, indicating the attraction between Cu^{2+} and -NH_2 of d-CDs. UV spectra of d-CDs in the presence of Cu^{2+} ions indicate the rise of a new peak of 438 nm, indicating the static complex formation -NH_2 of d-CDs with an LOD of 44.63 nmol/L and visual color change from pale yellow to orange. The quenching of the EM peak at 360 nm occurs because of through-bond energy transfer (TBET). Li and colleagues created reduced carbon dots (re-CDs) that exhibit two EM peaks at 650 and 680 nm, enabling the precise differentiation and detection of zinc (Zn^{2+}) and manganese (Mn^{2+}) ions. [150]. As the concentration of zinc ions (Zn^{2+}) was raised in the presence of reduced carbon dots (re-CDs), there was an observed increase in emission intensity at 650 nm and a corresponding decrease at 680 nm. Conversely, the introduction of manganese ions (Mn^{2+}) resulted in a diminished intensity at 650 nm, while the intensity at 680 nm remained unchanged. The limits of detection (LOD) for Zn^{2+} and Mn^{2+} were determined to be 9.09 nmol/L and 0.932 nmol/L, respectively.

5.5 Green carbon dots

CDs sourced from natural precursors exhibit advantages such as excellent solubility in water, biocompatibility, and less toxicity. Even though producing CDs from natural precursors exhibits various difficulties, it is widely used because of its numerous benefits such as pollution-free synthesis, less cost of synthesis, sustainability, high activity, extremely small size, and large surface area [151]. Due to these numerous advantages of green CDs, it is widely used in various applications such as FL imaging, drug delivery, photovoltaics, and catalysis. Green CDs have attained great development in the field of sensors due to their natural precursors, which are heteroatoms such as nitrogen, oxygen, sulfur, and chlorine. These green CDs possess stable properties and high QY without any passivation procedures [152]. Mercy et al. synthesized a green carbon quantum dot using rice husk via a one-pot synthesis route [153]. The synthesized carbon quantum dots exhibited band gap values in the range of 3.2 eV and were employed in the detection of

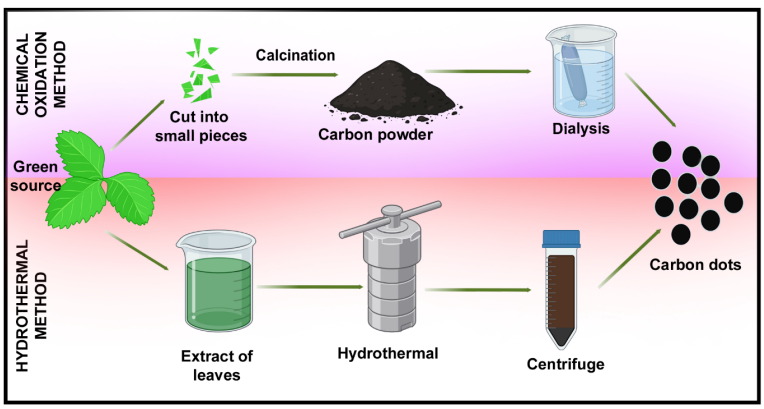

Figure 6. Major synthesis routes of carbon dot from natural resources.

antibiotics. Chemical oxidation and hydrothermal synthesis are two widely used methods to prepare green carbon dots, as shown in Figure 6.

6. Future perspectives and challenges

Looking ahead, several exciting future perspectives emerge in CDs for HM sensing. Firstly, further research into the fundamental understanding of CDs' structure-property relationships and complex formation mechanisms with HMs will pave the way for the rational design of CDs with enhanced sensing capabilities. This includes exploring novel synthesis routes, surface functionalization strategies, and doping techniques to tailor CDs for improved sensitivity, selectivity, and stability toward specific HMs. Furthermore, exploring novel applications beyond traditional sensing, such as imaging-guided therapy and environmental remediation, showcases the versatility and multifaceted utility of CDs. Collaborative efforts between materials scientists, chemists, biologists, and environmental engineers will drive the translation of CDs-based sensing technologies from the laboratory to practical field applications, addressing critical challenges in environmental monitoring, industrial safety, and public health. A range of less explored sustainable precursors, including recycled waste, biomaterials, and residues, should be evaluated for producing naturally doped CDs with high quantum yield. Besides gaining a mechanistic understanding of the formation of green CDs, it is essential to determine the reasons behind the precursor-based specificity of CDs toward certain metal ions. Moreover, implementing simple and simultaneous surface modifications could improve the optical signal for better applicability. Extensive studies are needed to create ratiometric and reusable sensing probes with surface modifications that emit fluorescence in the UV-visible-NIR region.

7. Conclusion

In conclusion, the burgeoning field of CDs holds immense promise for HMs sensing applications. HMs in the environment cause severe health issues to terrestrial and aquatic organisms. Through meticulous exploration of their synthesis methods, surface functionalization strategies, and intricate, complex formation mechanisms, researchers have unlocked the potential of CDs as highly sensitive and selective sensors for HMs. The versatile nature of CDs, coupled with their tunable optical properties, surface properties, and biocompatibility, renders them ideal candidates for addressing the pressing need for efficient and reliable HMs detection in diverse environmental and biomedical sensing. Ratiometric sensing presents benefits compared to traditional fluorescence and colorimetric sensing by mitigating background interferences. Leveraging the strengths of green precursor-derived carbon dots for heavy metal sensing amplifies these advantages.

Supplementary Tables

Table 1. Recent studies on nanomaterials for sensing heavy metals via the fluorometric technique.

S.No	Nanomaterials	Synthesis route	Size (nm)	LOD	Metal ions	Ref
1	Nanofiber/Fe/CDs nanocomposite	Sono chemical /Hydrothermal	30	-	Mercury and lead	[154]
2	N, S doped graphene QDs	Green pyrolysis method	3.15	0.69 (nm)	Mercury	[155]
3	Blue and red dual channel dual EMcarbon dots	One-step Hydrothermal method	2.5	27 and 34 (nm)	Chromium and lead	[156]
4	Blue-luminescent CDs	Pyrolysis method	10	$0.708-2.4$ (ppb)	Chromium	[157]
5	N, P Doped CDs	Hydrothermal method	$2.46-5.95$	26 (nm)	Chromium	[158]
6	CDs and boron CDs	One-step microwave-assisted method	7.2 ± 1.2	1-96 (nm)	Copper, Iron, Mercury, and lead	
7	Holmium-doped carbon dot-gelatin nanoparticles	Two-step desolvation method	49.5 ± 15.76	0.01 (μM)	Copper	[159]
8	Microline CDs nanostructure	Hydrothermal method	3-4	4 (μM)	Chromium and iron	[160]
9	N-Doped CDs	Hydrothermal method	-	0.31 and 56 (nm)	Iron and copper	[124]
10	Carbon dot decorated boehmite nanostructure	In-situ Hydrothermal method	-	66 (nm)	Chromium	[161]
11	CDs	Hydrothermal method	3	0.70 (μM)	Iron	[162]

Table 2. Recent studies on nanomaterials for sensing Heavy Metals via a colorimetric technique.

S. No	Nanomaterials	Heavy metals	LOD	Linear range(LR)	Colour change	Ref
1	(Mpd-CDS)	Iron	2.98 (μM)	0.56 – 2.98 (μM)	Colorless to reddish brown color	[163]
2	GSH Capped Syzygium cumini CDs	Lead Iron Manganese	0.13, 2.5, 2.1 (μM)	0.005 – 0.075, 0.0075 – 0.01, 0.0075 – 0.1 (μM)	Colorless to white Colorless to Brown Colorless to Dark brown	[164]
3	AuNPs@CDs	Mercury	3.7 (nM)	7 – 150 (nM)	Light blue to dark blue	[165]
4	CD	Iron	0.29 (μM)	-	Mauve to orange	[166]
5	(SN-CDs/AuNPs)	Mercury	0.5 (μM)	0.5 – 4.0 (μM)	Wine red to bluish violet	[167]
6	CQDs-TiO_2	Fluoride	2 (ppm)	2 – 8 (ppm)	Green to black	[168]
7	Carbon dots and SiO_2	Silver	1.6 (nM)	0.001-1000 (nM)	Blue to purple and then pink	[169]
8	(Agr/CD) hydrogel film	Chromium Lead Manganese	1 (pm) 0.5, 0.5 (nM)	-	Colourless to yellow Colourless to white Colourless to Tan brown	[170]

Table 3. Types of Carbon dots in ratiometric sensing of heavy metal ions.

Types of CDs	Carbon dots (λ_{em})	Functionalization (λ_{em})	Metals detected	LOD	LR	Color change	Ref
Metal nanocluster hybridized CDs	CDs (450 nm)	Glutathione Copper nanoclusters (750 nm)	Dichromate ions (Cr2O72) and Cadmium ions (Cd^{2+})	0.9, 2.3 μmol/L	0 – 120, 12.5 – 200 μmol/L	Yellow-green to Green Yellow-green to Pink	[171]
	CDs (450 nm)	Copper nanoclusters (647 nm)	Mercury (Hg^{2+})	0.31 nmol/L	-	Pink to Blue	[172]
	Blue Blue CDs (452 nm)	Bovine Serum albumin albumin-modified gold nanoclusters (BSA-Au NC) (654 nm)	Copper ions (Cu^{2+})	16 nM	0.05 – 1.85 μM	red to pink to purple to blue	[173]
Metal-organic frameworks-doped CDs	CDs (430nm)	Europium-MOFs (614 nm)	Mercury (Hg^{2+})	0.12 nM	0 – 300 μM	-	[174]
	CDs (458 nm)	Europium-Zeolitic imidazolate Framework-8 (ZIF-8) (612 nm)	Iron (Fe^{3+})	0.897 μM	0 – 6 μM	-	[175]
	CDs (460 nm)	Zeolitic imidazolate Framework-8 (ZIF-8) (560 nm)	Copper ions (Cu^{2+})	11.712 μM	-	-	[176]
Dual emissive CDs	Dual emissive CDs (500,678 nm)	-	Mercury (Hg^{2+})	6.25 nm	-	Blue to pink	[177]
	N, S doped Dual emissive CDs (416,688 nm)	-	Iron (Fe^{3+})	83 nm	0.1 – 40 μm	-	[178]
	Dual emissive CDs (465,535 nm)	-	Chromium (Cr (VI))	0.41 μM	-	-	[179]
Quantum dots doped CDs	CDs (445 nm)	Cerium-doped Cadmium telluride (CdTe) quantum dots (599 nm)	Mercury (Hg^{2+})	2.63 nm/L	1 – 60 nm	-	[180]
	Hydrophilic carbon nanodots (CD) (490 nm)	Quantum dots @ amphiphilic polyurethane (QD@PU) (621 nm)	Mercury (Hg^{2+})	10.5 nm	0.5 – 10 μm	-	[181]
Lanthanide ions hybridized CDs	N, S Codoped Carbon quantum dots (443 nm)	Ad-Eu-DPA (Adenine-Europium ions (Eu^{3+})-Dipicolinic acid) (617 nm)	Mercury (Hg^{2+})	0.2 nm	0.001 – 0.02 μM	Strong blue to light blue to lavender to deep purple	[182]
	CDs (415 nm)	AMP-Tb-Phen (Adensoine mono phosphate-Terbium- phenanthroline) (548 nm)	Fe^{2+} Fe^{3+} Ascorbic acid	50 nM- 100 μM, 100 nM-80 μM 0.5 μM to 150 μM	23 nM 88 nm 0.19 μM	-	[183]

Table 4. Green synthesized CDs for various metal sensing.

S. No	Source	Synthesis route	Metals detected	Detection Limit	Linearity range	Quantum yield	Ref
1.	Cassava pulp	Hydrothermal Method	Hg^{2+} Cu^{2+} Fe^{3+}	12, 21.7, 11.2 μM	30 – 600, 0 – 200, 0 – 250 μM	NA	[184]
2.	Kentucky Bluegrass	Hydrothermal Method	Mn^{2+} Fe^{3+}	1.2, 1.4 μM	5 – 25 μM	7%	[185]
3.	Agar	Hydrothermal Method	Fe^{3+}	75 nM	0.5 – 1500 μM	32%	[186]
4.	Mango leaves	Pyrolysis Method	Fe^{2+}	0.62 ppm	0 – 1000 μL	18.2%	[187]
5.	Seville orange	Hydrothermal Method	Fe^{3+}	0.53 μM	0.033 – 0.133 mM	13.3%	[188]
6.	Citrus lemon	Hydrothermal Method	Hg^{2+}	18.3 nM	0 – 100 μM	31%	[189]
7.	Extract of 12 different orange peel	Hydrothermal Method	Cr (VI)	0.8 μM	10 nM-50 μM	18.57%	[190]
8.	Maple tree leaves	Hydrothermal Method	Cesium	160 nM	100 nM-100 μM	NA	[191]
9.	Paddy straw mushroom	Hydrothermal Method	Fe^{3+} Pb^{2+}	12, 16 nM	1 – 1000 μM	11.5 %	[192]
10.	Leaves of Catharanthus roseus	Hydrothermal Method	Al^{3+} Fe^{3+}	0.5, 0.3 μM	0 – 6, 0 – 6 μM	28.2%	[193]
11.	Banana juice	Hydrothermal Method	Cu^{2+}	0.3 μg mL^{-1}	0.3 μg mL^{-1}	32%	[194]
12.	Dwarf Banana peel	Hydrothermal Method	Fe^{3+}	0.66 μM	5 – 25 μM	23%	[195]
13.	Pine wood	Hydrothermal Method	Fe^{3+}	355.4 nmol	0 – 1000 mM	-	[196]
14.	Flax straw	Hydrothermal Method	CO^{2+} Cr6+ Ascorbic acid	0.38, 0.19, and 0.35 μM	0 – 500, 0.5 – 80, and 0 – 200 μM	20.7%	[197]
15.	Lychee waste	Solvothermal Method	Fe^{3+}	23.6 nM	0.1 – 1.6 μM	23.5%	[198]
16.	Kelp	Microwave irradiation	CO^{2+}	0.39 μM / L	1 – 200 μM / L	23.5%	[199]
17.	Dunaliella salina	Hydrothermal Method	Cr (VI) Hg^{2+}	0.018, 0.018 μM	0.03 – 0.20, 0.03 – 0.20 μM/L	8%	[200]
18.	Cranberry Beans	Hydrothermal Method	Fe^{3+}	9.55 μM	30 – 600 μM	10.85%	[201]
19.	Microalgae Biochar	Depolymerisation	Cu^{2+} Pb^{2+} Ni^{2+}	0.1, 0.01 and 0.1 μM	1.5 μM-10 mM, 0.01 μM-2 mM and 2.5 μM-10 mM	-	[202]
20.	Leaves of Prosopis juliflora	Carbonization	Hg^{2+} Chemet Drug	50, 10 ng/L	5 – 500, 2.5 – 22.5 ng/ml	5%	[203]

Authors Contributions
VK collected data and prepared an initial draft with the help of KH. AT and KG added more data and analyzed it further. AG was involved in the conception, design, additional data collection, and preparation of the final draft. All the authors have gone through the final draft and approved it.

Availability of Data and Materials
The data that support the findings of this study are available from the corresponding author upon reasonable request.

Conflict of Interests
The authors declare that they have no known competing financial interests or personal relationships that could have appeared to influence the work reported here.

References

[1] S. Šafranko, D. Goman, A. Stanković, M. Medvidović-Kosanović, T. Moslavac, I. Jerković, and S. Jokić. An overview of the recent developments in carbon quantum dots—promising nanomaterials for metal ion detection and (bio) molecule sensing. *Chemosensors*, **9**(6):138, 2021. DOI: https://doi.org/10.3390/chemosensors9060138.

[2] S. B. Shah. Heavy metals in the marine environment—an overview. *Springer, Cham.*, 2021. DOI: https://doi.org/10.1007/978-3-030-73613-2-1.

[3] S. Negahdari, M. Sabaghan, M. Pirhadi, M. Alikord, P. Sadighara, M. Darvishi, and M. Nazer. Potential harmful effects of heavy metals as a toxic and carcinogenic agent in marine food-an overview. *Egyptian Journal of Veterinary Sciences*, **52**(3):379–385, 2021. DOI: https://doi.org/10.21608/ejvs.2021.83716.1245.

[4] J. M. Vonnie, B. J. Ting, K. Rovina, N. M. N. Aqilah, K. W. Yin, and N. Huda. Natural and engineered nanomaterials for the identification of heavy Metal ions-A review. *Nanomaterials*, **12**(15):2665, 2022. DOI: https://doi.org/10.3390/nano12152665.

[5] M. Sobiech, P. Luliński, P. P. Wieczorek, and M. Marć. Quantum and carbon dots conjugated molecularly imprinted polymers as advanced nanomaterials for selective recognition of analytes in environmental, food and biomedical applications. *TrAC Trends in Analytical Chemistry*, **142**.

[6] S. Perumal, R. Atchudan, T. N. Jebakumar Immanuel Edison, S. Sangaraju, W. V. Sathyaraj, and Y. R. Lee. Water soluble PMPC-derived bright fluorescent nitrogen/phosphorous-doped carbon dots for fluorescent Ink (anti-counterfeiting) and cellular multicolor imaging. *Polymers*, **15**.

[7] Y. Hu, Z. Yang, X. Lu, J. Guo, R. Cheng, L. Zhu, C. F. Wang, and S. Chen. Facile synthesis of red dual-emissive carbon dots for ratiometric fluorescence sensing and cellular imaging. *Nanoscale*, **12**(9):5494–5500, 2020. DOI: https://doi.org/10.1039/D0NR00381F.

[8] G. Gedda, S. A. Sankaranarayanan, C. L. Putta, K. K. Gudimella, A. K. Rengan, and W. M. Girma. Green synthesis of multi-functional carbon dots from medicinal plant leaves for antimicrobial, antioxidant, and bioimaging applications. *Scientific Reports*, **13**(1): 6371, 2023. DOI: https://doi.org/10.1038/s41598-023-33652-8.

[9] M. Y. Pudza, Z. Z. Abidin, S. Abdul-Rashid, F. M. Yassin, A. S. M. Noor, and M. Abdullah. Synthesis and characterization of fluorescent carbon dots from tapioca. *ChemistrySelect*, **4**(14):4140–4146, 2019. DOI: https://doi.org/10.1002/slct.201900836.

[10] M. Y. Pudza, Z. Z. Abidin, S. Abdul-Rashid, F. M. Yasin, A. S. M. Noor, and J. Abdullah. Selective and simultaneous detection of cadmium, lead and copper by tapioca-derived carbon dot–modified electrode. *Environmental Science and Pollution Research*, **27**(12):13315–13324, 2020. DOI: https://doi.org/10.1007/s11356-020-07695-7.

[11] M. Abdullah Issa, Z. Z. Abidin, S. Sobri, S. Rashid, M. Adzir Mahdi, N. Y. Azowa Ibrahim, and M. Pudza. Facile synthesis of nitrogen-doped carbon dots from lignocellulosic waste. *Nanomaterials*, **9** (10), 2019.

[12] M. Yahaya Pudza, Z. Zainal Abidin, S. Abdul Rashid, F. Md Yasin, A. S. Noor, and M. A. Issa. Sustainable synthesis processes for carbon dots through response surface methodology and artificial neural network. *Processes*, **7**(10), 2019.

[13] M. S. Sankhla, R. Kumar, and P. Agrawal. Arsenic in water contamination & toxic effect on human health: Current scenario of India. *J Forensic Sci & Criminal Inves*, **10**(2):001–005, 2018. DOI: https://doi.org/10.19080/JFSCI.2018.10.555781.

[14] A. Patel, V. K. Chaudhary, A. Singh, D. Rai, and N. Patel. Pollution in river Ganga due to heavy metal toxicity and various mitigation plans-A Review. *Ecology Environment & Conservation*, **27**(1):382–393, 2021.

[15] A. E. Charkiewicz, W. J. Omeljaniuk, K. Nowak, M. Garley, and J. Nikliński. Cadmium toxicity and health effects-A brief summary. *Molecules*, **28**(18), 2023.

[16] I. Suhani, S. Sahab, V. Srivastava, and R. P. Singh. Impact of cadmium pollution on food safety and human health. *Current Opinion in Toxicology*, **27**:1–7, 2021. DOI: https://doi.org/10.1016/j.cotox.2021.04.004.

[17] K. Renu, R. Chakraborty, H. Myakala, R. Koti, A. C. Famurewa, H. Madhyastha, B. Vellingiri, A. George, and A. Valsala Gopalakrishnan. Molecular mechanism of heavy metals (Lead, Chromium, Arsenic, Mercury, Nickel and Cadmium) - induced hepatotoxicity - A review. *Chemosphere*, **271**:129735, 2021. DOI: https://doi.org/10.1016/j.chemosphere.2021.129735.

[18] S. Moitra, P. D. Blanc, and S. Sahu. Adverse respiratory effects associated with cadmium exposure in small-scale jewellery workshops in India. *Thorax*, **68**(6):565, 2013. DOI: https://doi.org/10.1136/thoraxjnl-2012-203029.

[19] T. Goyal, P. Mitra, P. Singh, S. Sharma, and P. Sharma. Assessement of blood lead and cadmium levels in occupationally exposed workers of Jodhpur, Rajasthan. *Indian Journal of Clinical Biochemistry*, **36**(1):100–107, 2021. DOI: https://doi.org/10.1007/s12291-020-00878-6.

[20] V. Bhardwaj, V. M. Nurchi, and S. K. Sahoo. Mercury toxicity and detection using chromo-fluorogenic Chemosensors. *Pharmaceuticals*, **14**(2):123, 2021. DOI: https://doi.org/10.3390/ph14020123.

[21] X. Wu, Y. Li, S. Yang, H. Tian, and B. Sun. A multiple-detection-point fluorescent probe for the rapid detection of mercury (II), hydrazine and hydrogen sulphide. *Dyes and Pigments*, **174**:108056, 2020. DOI: https://doi.org/10.1016/j.dyepig.2019.108056.

[22] M. Balali-Mood and M. Sadeghi. Toxic mechanisms of five heavy metals: mercury, lead, chromium, cadmium, and arsenic. *Frontiers in Pharmacology*, **12**:643972, 2021. DOI: https://doi.org/10.3389/fphar.2021.643972.

[23] M. K. Murthy, P. Khandayataray, C. S. Mohanty, and R. Pattanayak. A review on arsenic pollution, toxicity, health risks, and management strategies using nanoremediation approaches. *Reviews on Environmental Health*, (0), 2022. DOI: https://doi.org/10.1515/reveh-2022-0103.

[24] M. S. Sankhla, M. Kumari, M. Nandan, R. Kumar, and P. Agrawal. Heavy metals contamination in water and their hazardous effect on human health-a review. *Int. J. Curr. Microbiol. App. Sci.*, **5**(10):759–766, 2016. DOI: https://doi.org/10.2139/ssrn.3428216.

[25] M. L. Sall, A. K. D. Diaw, D. Gningue-Sall, S. Efremova Aaron, and J. J. Aaron. Toxic heavy metals: impact on the environment and human health, and treatment with conducting organic polymers, a review. *Environmental Science and Pollution Research*, **27**:29927–29942, 2020. DOI: https://doi.org/10.1007/s11356-020-09354-3.

[26] A. Singh, A. Sharma, R. K. Verma, R. L. Chopade, P. P. Pandit, V. Nagar, V. Aseri, S. K. Choudhary, G. Awasthi, and K. K. Awasthi. Heavy metal contamination of water and their toxic effect on living organisms. *The Toxicity of Environmental Pollutants*, , 2022. DOI: https://doi.org/10.5772/intechopen.105075.

[27] O. C. S. Al Hamouz and O. S. Akintola. Removal of lead and arsenic ions by a new series of aniline based polyamines. *Process Safety and Environmental Protection*, **106**:180–190, 2017. DOI: https://doi.org/10.1016/j.psep.2017.01.014.

[28] I. Khairul, Q. Q. Wang, Y. H. Jiang, C. Wang, and H. Naranmandura. Metabolism, toxicity and anticancer activities of arsenic compounds. *Oncotarget*, **8**(14):23905, 2017. DOI: https://doi.org/10.18632/oncotarget.14733.

[29] A. Kumar, A. M. M. S. C. P. Kumar, A. K. Chaturvedi, A. A. Shabnam, G. Subrahmanyam, R. Mondal, D. K. Gupta, S. K. Malyan, S. S. A. Kumar, S. Khan, and K. K. Yadav. Lead toxicity: health hazards, influence on food Chain, and sustainable remediation approaches. *International Journal of Environmental Research and Public Health*, **17**(7):2179, 2020. DOI: https://doi.org/10.3390/ijerph17072179.

[30] M. S. Collin, S. K. Venkatraman, N. Vijayakumar, V. Kanimozhi, S. M. Arbaaz, R. S. Stacey, J. Anusha, R. Choudhary, V. Lvov, and G. I. Tovar. Bioaccumulation of lead (Pb) and its effects on human: A review. *Journal of Hazardous Materials Advances*, **7**:100094, 2022. DOI: https://doi.org/10.1016/j.hazadv.2022.100094.

[31] D. R. Ortega, D. F. G. Esquivel, T. B. Ayala, B. Pineda, S. G. Manzo, J. M. Quino, P. C. Mora, and V. P. de la Cruz. Cognitive impairment induced by lead exposure during lifespan: Mechanisms of lead neurotoxicity. *Toxics*, **9**(2), 2021. DOI: https://doi.org/10.3390/toxics9020023.

[32] A. Mabrouk and H. B. Cheikh. Thymoquinone ameliorates lead-induced suppression of the antioxidant system in rat kidneys. *Libyan Journal of Medicine*, **11**(1):31018, 2016. DOI: https://doi.org/10.3402/ljm.v11.31018.

[33] Y. Zhan, S. He, X. Wan, J. Zhang, B. Liu, J. Wang, and Z. Li. Easy-handling bamboo-like polypyrrole nanofibrous mats with high adsorption capacity for hexavalent chromium removal. *Journal of Colloid and Interface Science*, **529**:385–395, 2018. DOI: https://doi.org/10.1016/j.jcis.2018.06.033.

[34] V. Laxmi and G. Kaushik. Toxicity of hexavalent chromium in environment, health threats, and its bioremediation and detoxification from tannery wastewater for environmental safety. *Bioremediation of Industrial Waste for Environmental Safety: Industrial Waste and its Management*, **1**:223–243, 2020. DOI: https://doi.org/10.1007/978-981-13-1891-7-11.

[35] A. Alengebawy, S. T. Abdelkhalek, S. R. Qureshi, and M. Q. Wang. Heavy metals and pesticides toxicity in agricultural soil and plants: Ecological risks and human health implications. *Toxics*, **9**(3):42, 2021. DOI: https://doi.org/10.3390/toxics9030042.

[36] Q. Zhang, Q. Hou, G. Huang, and Q. Fan. Removal of heavy metals in aquatic environment by graphene oxide composites: A review. *Environmental Science and Pollution Research*, **27**:190–209, 2020. DOI: https://doi.org/10.1007/s11356-019-06683-w.

[37] S. Khatua and S. K. Dey. The chemistry and toxicity of chromium pollution: An overview. *Asian J. Agric. Hortic. Res.*, **10**(2):1–14, 2023. DOI: https://doi.org/10.9734/AJAHR/2023/v10i2221.

[38] G. A. Atiya Ali and M. N. Abbas. Atomic spectroscopy technique employed to detect the heavy metals from Iraqi waterbodies using natural BioFilter (Eichhornia crassipes): Thera dejla as a case study. *Systematic Reviews in Pharmacy*, **11**(9), 2020.

[39] J. Sardans, F. Montes, and J. Peñuelas. Determination of As, Cd, Cu, Hg and Pb in biological samples by modern electrothermal atomic absorption spectrometry. *Spectrochimica Acta Part B: Atomic Spectroscopy*, **65**(2):97–112, 2010. DOI: https://doi.org/10.1016/j.sab.2009.11.009.

[40] W. Chen, Y. Yang, K. Fu, D. Zhang, and Z. Wang. Progress in ICP-MS analysis of minerals and heavy metals in traditional medicine. *Frontiers in Pharmacology*, **13**:891273, 2022. DOI: https://doi.org/10.3389/fphar.2022.891273.

[41] M. Moldovan, E. M. Krupp, A. E. Holliday, and O. F. X. Donard. High resolution sector field ICP-MS and multicollector ICP-MS as tools for trace metal speciation in environmental studies: a review. *Journal of Analytical Atomic Spectrometry*, **19**(7):815–822, 2004. DOI: https://doi.org/10.1039/B403128H.

[42] T. M. Adeniji and K. J. Stine. Nanostructure modified electrodes for electrochemical detection of contaminants of emerging concern. *Coatings*, **13**(2):381, 2023. DOI: https://doi.org/10.3390/coatings13020381.

[43] C. Guo, L. Lv, Y. Liu, M. Ji, E. Zang, Q. Liu, M. Zhang, and M. Li. Applied analytical methods for detecting heavy metals in medicinal plants. *Critical Reviews in Analytical Chemistry*, **53**(2):339–359, 2023. DOI: https://doi.org/10.1080/10408347.2021.1953371.

[44] X. Sui, J. R. Downing, M. C. Hersam, and J. Chen. Additive manufacturing and applications of nanomaterial-based sensors. *Materials Today*, **48**:135–154, 2021. DOI: https://doi.org/10.1016/j.mattod.2021.02.001.

[45] R. Pavadai, A. Amalraj, S. Subramanian, and P. Perumal. High catalytic activity of Fluorophore-Labeled Y-shaped DNAzyme/3D MOF-MoS2NBs as a versatile biosensing platform for the simultaneous detection of Hg^{2+}, Ni^{2+}, and Ag^{+} ions. *ACS Applied Materials & Interfaces*, **13**(27):31710–31724, 2021. DOI: https://doi.org/10.1021/acsami.1c07086.

[46] A. Amalraj, R. Pavadai, and P. Perumal. Recyclable Target Metal-Enhanced Fluorometric Naked Eye Aptasensor for the Detection of Pb^{2+} and Ag^{+} Ions Based on the Structural Change of $CaSnO_3$@PDANS-Constrained GC-Rich ssDNA. *ACS Omega*, **6**(45):30580–30597, 2021. DOI: https://doi.org/10.1021/acsomega.1c04319.

[47] A. Amalraj, M. Narayanan, and P. Perumal. Highly efficient peroxidase-like activity of a metal–oxide-incorporated CeO2–MIL(Fe) metal–organic framework and its application in the colorimetric detection of melamine and mercury ions via induced hydrogen and covalent bonds. *Analyst*, **147**(14):3234–3247, 2022. DOI: https://doi.org/10.1039/D2AN00864E.

[48] A. Amalraj and P. Perumal. Dual fluorometric biosensor based on a nanoceria encapsulated metal organic framework and a signal amplification strategy of a hybridization chain reaction for the detection of melamine and Pb^{2+} ions in food samples. *New Journal of Chemistry*, **46**(27):12952–12967, 2022. DOI: https://doi.org/10.1039/D2NJ01089E.

[49] P. Shao, D. Liang, L. Yang, H. Shi, Z. Xiong, L. Ding, X. Yin, K. Zhang, and X. Luo. Evaluating the adsorptivity of organo-functionalized silica nanoparticles towards heavy metals: Quantitative comparison and mechanistic insight. *Journal of Hazardous Materials*, **387**:121676, 2020. DOI: https://doi.org/10.1016/j.jhazmat.2019.121676.

[50] P. Pallavi, K. Harini, S. Alshehri, M. M. Ghoneim, A. Alshlowi, P. Gowtham, K. Girigoswami, F. Shakeel, and A. Girigoswami.

[51] L. Laskowski, M. Laskowska, N. Vila, M. Schabikowski, and A. Walcarius. Mesoporous silica-based materials for electronics-oriented applications. *Molecules*, **24**(13):2395, 2019. DOI: https://doi.org/10.3390/molecules24132395.

[52] M. Hasanpour and M. Hatami. Application of three dimensional porous aerogels as adsorbent for removal of heavy metal ions from water/wastewater: A review study. *Advances in Colloid and Interface Science*, **284**:102247, 2020. DOI: https://doi.org/10.1016/j.cis.2020.102247.

[53] A. Sharma, M. Majdinasab, R. Khan, Z. Li, A. Hayat, and J. L. Marty. Nanomaterials in fluorescence-based biosensors: Defining key roles. *Nano-Structures & Nano-Objects*, **27**:100774, 2021. DOI: https://doi.org/10.1016/j.nanoso.2021.100774.

[54] X. P. Kong, B. H. Zhang, and J. Wang. Multiple roles of mesoporous silica in safe pesticide application by nanotechnology: A review. *Journal of Agricultural and Food Chemistry*, **69**(24):6735–6754, 2021. DOI: https://doi.org/10.1021/acs.jafc.1c01091.

[55] M. Santhamoorthy, A. Mohan, K. S. Mani, T. Devendhiran, G. Periyasami, S. C. Kim, M. C. Lin, K. Kumarasamy, P. J. Huang, and A. Ali. Synthesis of functionalized mesoporous silica nanoparticles for colorimetric and fluorescence sensing of selective metal (Fe^{3+}) ions in aqueous solution. *Methods*, **223**:26–34, 2024. DOI: https://doi.org/10.1016/j.ymeth.2024.01.010.

[56] M. C. Stoian, I. Mihalache, M. Matache, and A. Radoi. Terbium-functionalized silica nanoparticles for metal ion sensing by fluorescence quenching. *Dyes and Pigments*, **187**:109144, 2021. DOI: https://doi.org/10.1016/j.dyepig.2021.109144.

[57] K. Srinivasan, K. Subramanian, A. Rajasekar, K. Murugan, G. Benelli, and K. Dinakaran. A sensitive optical sensor based on DNA-labelled Si@ SiO_2 core–shell nanoparticle for the detection of Hg^{2+} ions in environmental water samples. *Bulletin of Materials Science*, **40**:1455–1462, 2017. DOI: https://doi.org/10.1007/s12034-017-1486-x.

[58] Y. N. Cetinkaya, O. Bulut, H. A. Oktem, and M. D. Yilmaz. Fluorescent silica nanoparticles as nano-chemosensors for the sequential detection of Pb^{2+} ions and bacterial-spore biomarker dipicolinic acid (DPA) in aqueous solution. *Spectrochimica Acta Part A: Molecular and Biomolecular Spectroscopy*, **303**:123222, 2023. DOI: https://doi.org/10.1016/j.saa.2023.123222.

[59] P. Fathima Fasna and S. Sasi. A comprehensive overview on advanced sensing applications of functional metal organic frameworks (MOFs). *Chemistry Select*, **6**(25):6365–6379, 2021. DOI: https://doi.org/10.1002/slct.202101533.

[60] Y. K. Li, T. Yang, M. L. Chen, and J. H. Wang. Recent advances in nanomaterials for analysis of trace heavy metals. *Critical Reviews in Analytical Chemistry*, **51**(4):353–372, 2021. DOI: https://doi.org/10.1080/10408347.2020.1736505.

[61] G. R. Xu, Z. H. An, K. Xu, Q. Liu, R. Das, and H. L. Zhao. Metal organic framework (MOF)-based micro/nanoscaled materials for heavy metal ions removal: The cutting-edge study on designs, synthesis, and applications. *Coordination Chemistry Reviews*, **427**:213554, 2021. DOI: https://doi.org/10.1016/j.ccr.2020.213554.

[62] M. B. Nguyen, D. T. N. Nga, V. T. Thu, B. Piro, T. N. P. Truong, P. T. H. Yen, G. H. Le, L. Q. Hung, T. A. Vu, and V. T. T. Ha. Novel nanoscale Yb-MOF used as highly efficient electrode for simultaneous detection of heavy metal ions. *Journal of Materials Science*, **56**:8172–8185, 2021. DOI: https://doi.org/10.1007/s10853-021-05815-3.

[63] S. S. Hossain, V. Karthik, A. Dhakshinamoorthy, and S. Biswas. A recyclable MOF@ polymer thin film composite for nanomolar on-site fluorometric detection of heavy metal ion and anti-histamine drug and efficient heterogeneous catalysis of Friedel–Crafts alkylation. *Inorganic Chemistry Frontiers*, **11**(1):142–155, 2024. DOI: https://doi.org/10.1039/D3QI01890C.

[64] A. A. Ansari, A. M. Khan, M. A. S. Salem, and A. S. Bhat. Synthesis and characterization of Ni@UiO-66 Metal-Organic Framework for fluorescence detection of heavy metal ions in the aqueous phase. *Materials Chemistry and Physics*, **318**:129245, 2024. DOI: https://doi.org/10.1016/j.matchemphys.2024.129245.

[65] K. Harini, K. Girigoswami, P. Pallavi, P. Gowtham, A. D. Prabhu, and A. Girigoswami. Advancement of magnetic particle imaging in diagnosis and therapy. *Advances in Natural Sciences: Nanoscience and Nanotechnology*, **15**(2):023002, 2024. DOI: https://doi.org/10.1088/2043-6262/ad3b7a.

[66] G. Amsaveni, A. S. Farook, V. Haribabu, R. Murugesan, and A. Girigoswami. Engineered multifunctional nanoparticles for DLA cancer cells targeting, sorting, MR imaging and drug delivery. *Advanced Science, Engineering and Medicine*, **5**(12):1340–1348, 2013. DOI: https://doi.org/10.1166/asem.2013.1425.

[67] V. Haribabu, A. S. Farook, N. Goswami, R. Murugesan, and A. Girigoswami. Optimized Mn-doped iron oxide nanoparticles entrapped in dendrimer for dual contrasting role in MRI. *Journal of Biomedical Materials Research Part B: Applied Biomaterials*, **104**(4):817–824, 2016.

[68] K. Zargoosh, H. Abedini, A. Abdolmaleki, and M. R. Molavian. Effective removal of heavy metal ions from industrial wastes using Thiosalicylhydrazide-modified magnetic nanoparticles. *Industrial & Engineering Chemistry Research*, **52**(42):14944–14954, 2013. DOI: https://doi.org/10.1021/ie401971w.

[69] A. Bilgic and A. Cimen. A highly sensitive and selective ON-OFF fluorescent sensor based on functionalized magnetite nanoparticles for detection of Cr(VI) metal ions in the aqueous medium. *Journal of Molecular Liquids*, **312**:113398, 2020. DOI: https://doi.org/10.1016/j.molliq.2020.113398.

[70] N. Tejwan, S. K. Saha, and J. Das. Multifaceted applications of green carbon dots synthesized from renewable sources. *Advances in Colloid and Interface Science*, **275**:102046, 2020. DOI: https://doi.org/10.1016/j.cis.2019.102046.

[71] P. Gowtham, K. Girigoswami, A. D. Prabhu, P. Pallavi, A. Thirumalai, K. Harini, and A. Girigoswami. Hydrogels of alginate derivative-encased nanodots featuring carbon-coated manganese ferrite cores with gold shells to offer antiangiogenesis with multimodal imaging-based theranostics. *Advanced Therapeutics*, :2400054, 2024. DOI: https://doi.org/10.1002/adtp.202400054.

[72] P. Gowtham, K. Harini, A. Thirumalai, P. Pallavi, K. Girigoswami, and A. Girigoswami. Synthetic routes to theranostic applications of carbon-based quantum dots. *ADMET and DMPK*, **11**(4):457–485, 2023. DOI: https://doi.org/10.5599/admet.1747.

[73] R. B. González-González, M. B. Morales-Murillo, M. A. Martínez-Prado, E. M. Melchor-Martínez, I. Ahmed, M. Bilal, R. Parra-Saldívar, and H. M. Iqbal. Carbon dots-based nanomaterials for fluorescent sensing of toxic elements in environmental samples: Strategies for enhanced performance. *Chemosphere*, **300**:134515, 2022. DOI: https://doi.org/10.1016/j.chemosphere.2022.134515.

[74] P. Li and S. F. Li. Recent advances in fluorescence probes based on carbon dots for sensing and speciation of heavy metals. *Nanophotonics*, **10**(2):877–908, 2020. DOI: https://doi.org/10.1515/nanoph-2020-0507.

[75] S. D. T. Landa, N. K. R. Bogireddy, I. Kaur, V. Batra, and V. Agarwal. Heavy metal ion detection using green precursor derived carbon dots. *Iscience*, **25**(2), 2022. DOI: https://doi.org/10.1016/j.isci.2022.103816.

[76] P. Sharmiladevi, N. Akhtar, V. Haribabu, K. Girigoswami, S. Chattopadhyay, and A. Girigoswami. Excitation wavelength independent carbon-decorated ferrite nanodots for multimodal diagnosis and stimuli responsive therapy. *ACS Applied Bio Materials*, **2**(4):1634–1642, 2019. DOI: https://doi.org/10.1021/acsabm.9b00039.

[77] Q. Tan, X. Li, L. Wang, J. Zhao, Q. Yang, P. Sun, Y. Deng, and G. Shen. One-step synthesis of highly fluorescent carbon dots as fluorescence sensors for the parallel detection of cadmium and mercury ions. *Frontiers in Chemistry*, **10**:1005231, 2022. DOI: https://doi.org/10.3389/fchem.2022.1005231.

[78] D. Yoo, Y. Park, B. Cheon, and M. H. Park. Carbon dots as an effective fluorescent sensing platform for metal ion detection. *Nanoscale Research Letters*, **14**: 1–13, 2019. DOI: https://doi.org/10.1186/s11671-019-3088-6.

[79] T. Jaiganesh, J. Daisy Vimala Rani, and A. Girigoswami. Spectroscopically characterized cadmium sulfide quantum dots lengthening the lag phase of Escherichia coli growth. *Spectrochimica Acta Part A: Molecular and Biomolecular Spectroscopy*, **92**:29–32, 2012. DOI: https://doi.org/10.1016/j.saa.2012.02.044.

[80] A. Daulay, L. H. Nasution, M. Huda, M. Amin, and M. Nikmatullah. Green sources for carbon dots synthesis in sensing for food application–A review. *Biosensors and Bioelectronics*, :100460, 2024. DOI: https://doi.org/10.1016/j.biosx.2024.100460.

[81] P. Gowtham, K. Girigoswami, P. Pallavi, K. Harini, I. Gurubharath, and A. Girigoswami. Alginate-derivative encapsulated carbon coated manganese-ferrite nanodots for multimodal medical imaging. *Pharmaceutics*, **14**(12):2550, 2022. DOI: https://doi.org/10.3390/pharmaceutics14122550.

[82] Y. Wang, Y. Zhu, S. Yu, and C. Jiang. Fluorescent carbon dots: rational synthesis, tunable optical properties and analytical applications. *RSC Advances*, **7**(65):40973–40989, 2017. DOI: https://doi.org/10.1039/C7RA07573A.

[83] D. M. A. Crista, J. C. G. Esteves da Silva, and L. Pinto da Silva. Evaluation of Different Bottom-up Routes for the Fabrication of Carbon Dots. *Nanomaterials*, **10**(7):1316, 2020. DOI: https://doi.org/10.3390/nano10071316.

[84] K. Jiang, X. Gao, X. Feng, Y. Wang, Z. Li, and H. Lin. Carbon dots with dual-emissive, robust, and aggregation-induced room-temperature phosphorescence characteristics. *Angewandte Chemie International Edition*, **59**(3):1263–1269, 2020. DOI: https://doi.org/10.1002/anie.201911342.

[85] L. Yiye, F. Li, H. Xu, and G. Nie. Highly fluorescent chiral NS-doped carbon dots from cysteine: Affecting cellular energy metabolism. *Free Radical Biology and Medicine*, **165**:55, 2021. DOI: https://doi.org/10.1002/ange.201712453.

[86] J. Bhoopathy, W. V. Sathyaraj, L. Prabakaran, R. Senthil, V. Mohammed, and S. Dharmalingam. An investigation on bioderived sponges with Hemostatic and Photoluminescent properties for accelerating wound healing. *Journal of Polymers and the Environment*, 2024. DOI: https://doi.org/10.1007/s10924-024-03245-1.

[87] A. Girigoswami, W. Yassine, P. Sharmiladevi, V. Haribabu, and K. Girigoswami. Camouflaged nanosilver with excitation wavelength dependent high quantum yield for targeted theranostic. *Scientific Reports*, **8**(1):1–7, 2018. DOI: https://doi.org/10.1038/s41598-018-34843-4.

[88] F. Wang, Z. Xie, H. Zhang, C. Y. Liu, and Y. G. Zhang. Highly luminescent organosilane-functionalized carbon dots. *Advanced Functional Materials*, **21**(6):1027–1031, 2011. DOI: https://doi.org/10.1002/adfm.201002279.

[89] Z. Liu, H. Zou, N. Wang, T. Yang, Z. Peng, J. Wang, N. Li, and C. Huang. Photoluminescence of carbon quantum dots: coarsely adjusted by quantum confinement effects and finely by surface trap states. *Science China Chemistry*, **61**:490–496, 2018. DOI: https://doi.org/10.1007/s11426-017-9172-0.

[90] J. Yu, C. Liu, K. Yuan, Z. Lu, Y. Cheng, L. Li, X. Zhang, P. Jin, F. Meng, and H. Liu. Luminescence mechanism of carbon dots by tailoring functional groups for sensing Fe^{3+} ions. *Nanomaterials*, **8**(4):233, 2018. DOI: https://doi.org/10.3390/nano8040233Nanomaterials.

[91] Q. Fang, Y. Dong, Y. Chen, C. H. Lu, Y. Chi, H. H. Yang, and T. Yu. Luminescence origin of carbon based dots obtained from citric acid and amino group-containing molecules. *Carbon*, **118**:319–326, 2017. DOI: https://doi.org/10.1016/j.carbon.2017.03.061.

[92] M. L. Liu, B. B. Chen, C. M. Li, and C. Z. Huang. Carbon dots: synthesis, formation mechanism, fluorescence origin and sensing applications. *Green Chemistry*, **21**(3):449–471, 2019. DOI: https://doi.org/10.1039/C8GC02736F.

[93] S. Zhu, Y. Song, X. Zhao, J. Shao, J. Zhang, and B. Yang. The photoluminescence mechanism in carbon dots (graphene quantum dots, carbon nanodots, and polymer dots): current state and future perspective. *Nano Research*, **8**:355–381, 2015. DOI: https://doi.org/10.1007/s12274-014-0644-3.

[94] K. Jiang, S. Sun, L. Zhang, Y. Lu, A. Wu, C. Cai, and H. Lin. Red, green, and blue luminescence by carbon dots: full-color emission tuning and multicolor cellular imaging. *Angewandte Chemie*, **127**(18):5450–5453, 2015. DOI: https://doi.org/10.1002/ange.201501193.

[95] C. Liu, R. Wang, B. Wang, Z. Deng, Y. Jin, Y. Kang, and J. Chen. Orange, yellow and blue luminescent carbon dots controlled by surface state for multicolor cellular imaging, light emission and illumination. *Microchimica Acta*, **185**:1–8, 2018. DOI: https://doi.org/10.1007/s00604-018-3072-3.

[96] B. Yuan, S. Guan, X. Sun, X. Li, H. Zeng, Z. Xie, P. Chen, and S. Zhou. Highly efficient carbon dots with reversibly switchable green–red emissions for trichromatic white light-emitting diodes. *ACS Applied Materials & Interfaces*, **10**(18):16005–16014, 2018. DOI: https://doi.org/10.1021/acsami.8b02379.

[97] F. Yan, Z. Sun, H. Zhang, X. Sun, Y. Jiang, and Z. Bai. The fluorescence mechanism of carbon dots, and methods for tuning their emission color: a review. *Microchimica Acta*, **186**:1–37, 2019. DOI: https://doi.org/10.1007/s00604-019-3688-y.

[98] Y. Chen, H. Lian, Y. Wei, X. He, Y. Chen, B. Wang, Q. Zeng, and J. Lin. Concentration-induced multi-colored emissions in carbon dots: origination from triple fluorescent centers. *Nanoscale*, **10**(14):6734–6743, 2018. DOI: https://doi.org/10.1039/C8NR00204E.

[99] S. Yang, J. Sun, X. Li, W. Zhou, Z. Wang, P. He, G. Ding, X. Xie, Z. Kang, and M. Jiang. Large-scale fabrication of heavy doped carbon quantum dots with tunable-photoluminescence and sensitive fluorescence detection. *Journal of Materials Chemistry A*, **2**(23):8660–8667, 2014. DOI: https://doi.org/10.1039/C4TA00860J.

[100] X. Dong, L. Wei, Y. Su, Z. Li, H. Geng, C. Yang, and Y. Zhang. Efficient long lifetime room temperature phosphorescence of carbon dots in a potash alum matrix. *Journal of Materials Chemistry C*, **3**(12):2798–2801, 2015. DOI: https://doi.org/10.1039/C5TC00126A.

[101] R. A. Paynter, S. Wellons, and J. Winefordner. New method of analysis based on room-temperature phosphorescence. *Analytical Chemistry*, **46**(6):736–738, 1974. DOI: https://doi.org/10.1021/ac60342a044.

[102] X. Wei, J. Yang, L. Hu, Y. Cao, J. Lai, F. Cao, J. Gu, and X. Cao. Recent advances in room temperature phosphorescent carbon dots: preparation, mechanism, and applications. *Journal of Materials Chemistry C*, **9**(13):4425–4443, 2021. DOI: https://doi.org/10.1039/D0TC06031C.

[103] Q. Li, M. Zhou, M. Yang, Q. Yang, Z. Zhang, and J. Shi. Induction of long-lived room temperature phosphorescence of carbon dots by water in hydrogen-bonded matrices. *Nature Communications*, **9**(1):734, 2018. DOI: https://doi.org/10.1038/s41467-018-03144-9.

[104] Z. Tian, D. Li, E. V. Ushakova, V. G. Maslov, D. Zhou, P. Jing, D. Shen, S. Qu, and A. L. Rogach. Multilevel data encryption using thermal-treatment controlled room temperature phosphorescence of carbon dot/polyvinylalcohol composites. *Advanced Science*, **5**(9):1800795, 2018. DOI: https://doi.org/10.1002/advs.201800795.

[105] Q. Li, M. Zhou, Q. Yang, Q. Wu, J. Shi, A. Gong, and M. Yang. Efficient room-temperature phosphorescence from nitrogen-doped carbon dots in composite matrices. *Chemistry of Materials*, **28**(22):8221–8227, 2016. DOI: https://doi.org/10.1021/acs.chemmater.6b03049.

[106] C. Wang, Y. Chen, Y. Xu, G. Ran, Y. He, and Q. Song. Aggregation-induced room-temperature phosphorescence obtained from water-dispersible carbon dot-based composite materials. *ACS Applied Materials & Interfaces*, **12**(9):10791–10800, 2020. DOI: https://doi.org/10.1021/acsami.9b20500.

[107] Y. P. Sun, B. Zhou, Y. Lin, W. Wang, K. S. Fernando, P. Pathak, M. J. Meziani, B. A. Harruff, X. Wang, and H. Wang. Quantum-sized carbon dots for bright and colorful photoluminescence. *Journal of the American Chemical Society*, **128**(24):7756–7757, 2006. DOI: https://doi.org/10.1021/ja062677d.

[108] K. Dimos. Carbon quantum dots: surface passivation and functionalization. *Current Organic Chemistry*, **20**(6):682–695, 2016. DOI: https://doi.org/10.1002/smll.200700578.

[109] A. B. Bourlinos, A. Stassinopoulos, D. Anglos, R. Zboril, M. Karakassides, and E. P. Giannelis. Surface functionalized carbogenic quantum dots. *Small*, **4**(4):455–458, 2008. DOI: https://doi.org/10.1039/C4NJ01235F.

[110] T. Liu, N. Li, J. X. Dong, H. Q. Luo, and N. B. Li. Fluorescence detection of mercury ions and cysteine based on magnesium and nitrogen co-doped carbon quantum dots and IMPLICATION logic gate operation. *Sensors and Actuators B: Chemical*, **231**:147–153, 2016. DOI: https://doi.org/10.1016/j.snb.2016.02.141.

[111] C. Xie, L. Xiao, S. Peng, and X. Shi. Preparation of novel magnetic and fluorescent CS–Fe3O4@ CdSeS nanoparticles for simultaneous removal and optical determination of trace copper ions. *New Journal of Chemistry*, **38**(12):6095–6102, 2014. DOI: https://doi.org/10.1039/C4RA13820A.

[112] Y. Sun, C. Shen, J. Wang, and Y. Lu. Facile synthesis of biocompatible N, S-doped carbon dots for cell imaging and ion detecting. *RSC Advances*, **5**(21):16368–16375, 2015. DOI: https://doi.org/10.1039/C4RA13820A.

[113] S. Nong, M. Wang, X. Wang, Y. Li, S. Yu, C. Tang, G. Li, and L. Xu. A multifunctional guanosine-based carbon dots for dead microbial imaging and synergistic broad-spectrum antimicrobial therapy. *Chemical Engineering Journal*, page 150123, 2024. DOI: https://doi.org/10.1016/j.cej.2024.150123.

[114] W. Zhang, R. Wang, W. Liu, X. Wang, P. Li, W. Zhang, H. Wang, and B. Tang. Te-containing carbon dots for fluorescence imaging of superoxide anion in mice during acute strenuous exercise or emotional changes. *Chemical Science*, **9**(3):721–727, 2018. DOI: https://doi.org/10.1039/C7SC03878J.

[115] J. Du, S. Zhou, Y. Ma, Y. Wei, Q. Li, H. Huang, L. Chen, Y. Yang, and S. Yu. Folic acid functionalized gadolinium-doped carbon dots as fluorescence/-magnetic resonance imaging contrast agent for targeted imaging of liver cancer. *Colloids and Surfaces B: Biointerfaces*, **234**:113721, 2024. DOI: https://doi.org/10.1016/j.colsurfb.2023.113721.

[116] Y. Jiang, Z. Tan, T. Zhao, J. Wu, Y. Li, Y. Jia, and Z. Peng. Indocyanine green derived carbon dots with significantly enhanced properties for efficient photothermal therapy. *Nanoscale*, **15**(4):1925–1936, 2023. DOI: https://doi.org/10.1039/D2NR06058B.

[117] X. Shi, W. Wei, Z. Fu, W. Gao, C. Zhang, Q. Zhao, F. Deng, and X. Lu. Review on carbon dots in food safety applications. *Talanta*, **194**:809–821, 2019. DOI: https://doi.org/10.1016/j.talanta.2018.11.005.

[118] K. Radhakrishnan, S. Sivanesan, and P. Panneerselvam. Turn-On fluorescence sensor based detection of heavy metal ion using carbon dots@graphitic-carbon nitride nanocomposite probe. *Journal of Photochemistry and Photobiology A: Chemistry*, **389**:112204, 2020. DOI: https://doi.org/10.1016/j.jphotochem.2019.112204.

[119] X. Zhao, X. Zhang, Q. Li, Y. Song, J. Zhang, Y. Yang, X. Xia, and Q. Han. Rapid determination of cadmium in Panax notoginseng using NCDs quantum carbon dots-aptamer fluorescence sensor. *Journal of Food Measurement and Characterization*, **16**(4):2459–2467, 2022. DOI: https://doi.org/10.1007/s11694-022-01356-8.

[120] B. Wang and S. Lu. The light of carbon dots: From mechanism to applications. *Matter*, **5**(1):110–149, 2022. DOI: https://doi.org/10.1016/j.matt.2021.10.016.

[121] V. Can, B. Onat, E. S. Cirit, F. Sahin, and Z. C. Canbek Ozdil. Metal-Enhanced Fluorescent Carbon Quantum Dots via One-Pot Solid State Synthesis for Cell Imaging. *ACS Applied Bio Materials*, **6**(5):1798–1805, 2023. DOI: https://doi.org/10.1021/acsabm.3c00040.

[122] H. Wang, L. Ai, H. Song, Z. Song, X. Yong, S. Qu, and S. Lu. Innovations in the Solid-State Fluorescence of Carbon Dots: Strategies, Optical Manipulations, and Applications. *Advanced Functional Materials*, **33**(41):2303756, 2023. DOI: https://doi.org/10.1002/adfm.202303756.

[123] M. Batool, H. M. Junaid, S. Tabassum, F. Kanwal, K. Abid, Z. Fatima, and A. T. Shah. Metal ion detection by carbon dots-a review. *Critical Reviews in Analytical Chemistry*, **52**(4):756–767, 2022. DOI: https://doi.org/10.1080/10408347.2020.1824117.

[124] R. Bandi, R. Dadigala, B. R. Gangapuram, F. K. Sabir, M. Alle, S. H. Lee, and V. Guttena. N-Doped carbon dots with pH-sensitive emission, and their application to simultaneous fluorometric determination of iron(III) and copper(II). *Microchimica Acta*, **187** (1):30, 2019. DOI: https://doi.org/10.1007/s00604-019-4017-1.

[125] S. K. Panigrahi and A. K. Mishra. Inner filter effect in fluorescence spectroscopy: As a problem and as a solution. *Journal of Photochemistry and Photobiology C: Photochemistry Reviews*, **41**:100318, 2019. DOI: https://doi.org/10.1016/j.jphotochemrev.2019.100318.

[126] H. Shabbir, E. Csapó, and M. Wojnicki. Carbon quantum dots: the role of surface functional groups and proposed mechanisms for metal ion sensing. *Inorganics*, **11**(6):262, 2023. DOI: https://doi.org/10.3390/inorganics11060262.

[127] C. Sakdaronnarong, A. Sangjan, S. Boonsith, D. C. Kim, and H. S. Shin. Recent developments in synthesis and photocatalytic applications of carbon dots. *Catalysts*, **10**(3):320, 2020. DOI: https://doi.org/10.3390/catal10030320.

[128] Y. Z. Fan, Y. Zhang, N. Li, S. G. Liu, T. Liu, N. B. Li, and H. Q. Luo. A facile synthesis of water-soluble carbon dots as a label-free fluorescent probe for rapid, selective and sensitive detection of picric acid. *Sensors and Actuators B: Chemical*, **240**:949–955, 2017. DOI: https://doi.org/10.1016/j.snb.2016.09.063.

[129] P. Li and S. F. Y. Li. Recent advances in fluorescence probes based on carbon dots for sensing and speciation of heavy metals. *Nanophotonics*, **10**(2):877–908, 2021. DOI: https://doi.org/10.1515/nanoph-2020-0507.

[130] L. C. Zhang, Y. M. Yang, L. Liang, Y. J. Jiang, C. M. Li, Y. F. Li, L. Zhan, H. Y. Zou, and C. Z. Huang. Lighting up of carbon dots for copper(ii) detection using an aggregation-induced enhanced strategy. *Analyst*, **147**(3):417–422, 2022. DOI: https://doi.org/10.1039/D1AN02147H.

[131] S. Carter, R. Clough, A. Fisher, B. Gibson, and B. Russell. Atomic spectrometry update: review of advances in the analysis of metals, chemicals and materials. *Journal of Analytical Atomic Spectrometry*, **37**(11):2207–2281, 2022. DOI: https://doi.org/10.1039/C3JA90051G.

[132] S. l. Zhou, S. m. Zhang, and H. g. Li. Carbon-dot-based solid-state luminescent materials: Synthesis and applications in white light emitting diodes and optical sensors. *New Carbon Materials*, **36**(3): 527–545, 2021. DOI: https://doi.org/10.1016/S1872-5805(21)60042-2.

[133] R. Mohan, J. Drbohlavova, and J. Hubalek. Dual band emission in carbon dots. *Chemical Physics Letters*, **692**:196–201, 2018. DOI: https://doi.org/10.1016/j.cplett.2017.12.029.

[134] M. Alfè, V. Gargiulo, M. Amati, V. A. Maraloiu, P. Maddalena, and S. Lettieri. Mesoporous TiO_2 from metal-organic frameworks for photoluminescence-based optical sensing of oxygen. *Catalysts*, **11**(7):795, 2021. DOI: https://doi.org/10.3390/catal11070795.

[135] L. Li and T. Dong. Photoluminescence tuning in carbon dots: surface passivation or/and functionalization, heteroatom doping. *Journal of Materials Chemistry C*, **6**(30):7944–7970, 2018. DOI: https://doi.org/10.1039/C7TC05878K.

[136] R. Pratap, N. Hassan, M. Yadav, S. K. Srivastava, S. Chaudhary, A. K. Verma, J. Lahiri, and A. S. Parmar. Biogenic synthesis of dual-emission chlorophyll-rich carbon quantum dots for detection of toxic heavy metal ions–Hg (ii) and As (iii) in water and mouse fibroblast cell line NIH-3T3. *Environmental Science: Nano*, 2024. DOI: https://doi.org/10.1039/D3EN00789H.

[137] H. Yuan, G. Yang, Q. Luo, T. Xiao, Y. Zuo, X. Guo, D. Xu, and Y. Wu. A 3D net-like structured fluorescent aerogel based on carboxy-methylated cellulose nanofibrils and carbon dots as a highly effective adsorbent and sensitive optical sensor of Cr (VI). *Environmental Science: Nano*, **7**(3):773–781, 2020. DOI: https://doi.org/10.1039/C9EN01394F.

[138] K. H. Gebremedhin, M. H. Kahsay, N. K. Wegahita, T. Teklu, B. A. Berhe, A. G. Gebru, A. H. Tesfay, and A. G. Asgedom. Nanomaterial-based optical colorimetric sensors for rapid monitoring of inorganic arsenic species: A review. *Discover Nano*, **19**(1): 38, 2024. DOI: https://doi.org/10.1186/s11671-024-03981-2.

[139] A. Aygun, I. Cobas, R. N. E. Tiri, and F. Sen. Hydrothermal synthesis of B, S, and N-doped carbon quantum dots for colorimetric sensing of heavy metal ions. *RSC Advances*, **14**(16):10814–10825, 2024. DOI: https://doi.org/10.1039/D4RA00397G.

[140] R. Bisauriya, S. Antonaroli, M. Ardini, F. Angelucci, A. Ricci, and R. Pizzoferrato. Tuning the sensing properties of N and S co-doped carbon dots for colorimetric detection of copper and cobalt in water. *Sensors*, **22**(7):2487, 2022. DOI: https://doi.org/10.3390/s22072487.

[141] H. Adam, S. C. Gopinath, M. M. Arshad, T. Adam, U. Hashim, Z. Sauli, M. A. Fakhri, S. Subramaniam, Y. Chen, and S. Sasidharan. Integration of microfluidic channel on electrochemical-based nanobiosensors for monoplex and multiplex analyses: An overview. *Journal of the Taiwan Institute of Chemical Engineers*, **146**:104814, 2023. DOI: https://doi.org/10.1016/j.jtice.2023.104814.

[142] D. Xiao, J. Zhai, Z. Shen, Q. Wang, S. Wei, Y. Li, and C Bian. A Novel Thin-Layer Flow Cell Sensor System Based on BDD Electrode for Heavy Metal Ion Detection. *Micromachines*, **15**(3):363, 2024. DOI: https://doi.org/10.3390/mi15030363.

[143] H. Song, M. Huo, M. Zhou, H. Chang, J. Li, Q. Zhang, Y. Fang, H. Wang, and D. Zhang. Carbon nanomaterials-based electrochemical sensors for heavy metal detection. *Critical Reviews in Analytical Chemistry*, :1–20, 2022. DOI: https://doi.org/10.1080/10408347.2022.2151832.

[144] Y. Zhang, D. Hou, Z. Wang, N. Cai, and C. Au. Nanomaterial-based dual-emission ratiometric fluorescent sensors for biosensing and cell imaging. *Polymers*, **13**(15):2540, 2012. DOI: https://doi.org/10.3390/polym13152540.

[145] A. Bigdeli, F. Ghasemi, S. Abbasi-Moayed, M. Shahrajabian, N. Fahimi-Kashani, S. Jafarinejad, M. A. F. Nejad, and M. R. Hormozi-Nezhad. Ratiometric fluorescent nanoprobes for visual detection: Design principles and recent advances-A review. *Analytica Chimica Acta*, **1079**:30–58, 2019. DOI: https://doi.org/10.1016/j.aca.2019.06.035.

[146] J. Liu, H. Xue, Y. Liu, T. Bu, P. Jia, Y. Shui, and L. Wang. Visual and fluorescent detection of mercury ions using a dual-emission ratiometric fluorescence nanomixture of carbon dots cooperating with gold nanoclusters. *Spectrochimica Acta Part A: Molecular and Biomolecular Spectroscopy*, **223**:117364, 2019. DOI: https://doi.org/10.1016/j.saa.2019.117364.

[147] F. Yarur, J. R. Macairan, and R. Naccache. Ratiometric detection of heavy metal ions using fluorescent carbon dots. *Environmental Science: Nano*, **6**(4):1121–1130, 2019. DOI: https://doi.org/10.1039/C8EN01418C.

[148] L. Wang, H. X. Cao, Y. S. He, C. G. Pan, T. K. Sun, X. Y. Zhang, C. Y. Wang, and G. X. Liang. Facile preparation of amino-carbon dots/gold nanoclusters FRET ratiometric fluorescent probe for sensing of Pb^{2+}/Cu^{2+}. *Sensors and Actuators B: Chemical*, **282**:78–84, 2019. DOI: https://doi.org/10.1016/j.snb.2018.11.058.

[149] G. Huang, X. Luo, X. He, Y. Han, H. Zhao, W. Tang, T. Yue, and Z. Li. Dual-emission carbon dots based ratiometric fluorescent sensor with opposite response for detecting copper (II). *Dyes and Pigments*, **196**:109803, 2021. DOI: https://doi.org/10.1016/j.dyepig.2021.109803.

[150] H. Li, X. Huang, F. Zhang, X. Luo, W. Yu, C. Li, B. Jiang, Z. Qiu, and Z. Xu. Specific discrimination of zinc and manganese ions by label free dual emissive carbon dots by ratiometric mode. *Talanta*, **260**:124627, 2023. DOI: https://doi.org/10.1016/j.talanta.2023.124627.

[151] S. Yadav and S Daniel. Green synthesis of zero-dimensional carbon nanostructures in energy storage applications—a Review. *Energy Storage*, **6**(1):e500, 2024. DOI: https://doi.org/10.1002/est2.500.

[152] X. Lin, M. Xiong, J. Zhang, C. He, X. Ma, H. Zhang, Y. Kuang, M. Yang, and Q. Huang. Carbon dots based on natural resources: Synthesis and applications in sensors. *Microchemical Journal*, **160**:105604, 2021. DOI: https://doi.org/10.1016/j.microc.2020.105604.

[153] D. J. Mercy, V. Kiran, A. Thirumalai, K. Harini, K. Girigoswami, and A. Girigoswami. Rice husk assisted carbon quantum dots synthesis for amoxicillin sensing. *Results in Chemistry*, **6**:101219, 2023. DOI: https://doi.org/10.1016/j.rechem.2023.101219.

[154] S. Ahmadian-Fard-Fini, D. Ghanbari, O. Amiri, and M. Salavati-Niasari. Electro-spinning of cellulose acetate nanofibers/Fe/carbon dot as photoluminescence sensor for mercury (II) and lead (II) ions. *Carbohydrate Polymers*, **229**:115428, 2020. DOI: https://doi.org/10.1016/j.carbpol.2019.115428.

[155] C. Qu, D. Zhang, R. Yang, J. Hu, and L. Qu. Nitrogen and sulfur co-doped graphene quantum dots for the highly sensitive and selective detection of mercury ion in living cells. *Spectrochimica Acta Part A: Molecular and Biomolecular Spectroscopy*, **206**:588–596, 2019. DOI: https://doi.org/10.1016/j.saa.2018.07.097.

[156] H. Lu, S. Xu, and J. Liu. One pot generation of blue and red carbon dots in one binary solvent system for dual channel detection of Cr^{3+} and Pb^{2+} based on ion imprinted fluorescence polymers. *ACS Sensors*, **4**(7):1917–1924, 2019. DOI: https://doi.org/10.1021/acssensors.9b00886.

[157] D. Pooja, L. Singh, A. Thakur, and P. Kumar. Green synthesis of glowing carbon dots from Carica papaya waste pulp and their application as a label-freechemo probe for chromium detection in water. *Sensors and Actuators B: Chemical*, **283**:363–372, 2019. DOI: https://doi.org/10.1016/j.snb.2018.12.027.

[158] J. Cai, G. Han, J. Ren, C. Liu, J. Wang, and X. Wang. Single-layered graphene quantum dots with self-passivated layer from xylan for visual detection of trace chromium (Vl). *Chemical Engineering Journal*, **435**:131833, 2022. DOI: https://doi.org/10.1016/j.cej.2021.131833.

[159] S. K. Bhattacharyya, I. D. Jana, N. Pandey, D. Biswas, A. Girigoswami, T. Dey, S. Banerjee, S. K. Ray, A. Mondal, and G. Mukherjee. Ho^{3+}-Doped Carbon dot/gelatin nanoparticles for pH-responsive anticancer drug delivery and intracellular Cu^{2+} Ion sensing. *ACS Applied Nano Materials*, **5**(8):11809–11822, 2022. DOI: https://doi.org/10.1021/acsanm.2c02841.

[160] S. Bardhan, S. Roy, D. K. Chanda, S. Ghosh, D. Mondal, S. Das, and S. Das. Nitrogenous carbon dot decorated natural microcline: an ameliorative dual fluorometric probe for Fe^{3+} and Cr^{6+} detection. *Dalton Transactions*, **49**(30):10554–10566, 2020. DOI: https://doi.org/10.1039/D0DT02166K.

[161] S. Roy, S. Bardhan, D. Mondal, I. Saha, J. Roy, S. Das, D. K. Chanda, P. Karmakar, and S. Das. Polymeric carbon dot/boehmite nanocomposite made portable sensing device (Kavach) for non-invasive and selective detection of Cr (VI) in wastewater and living cells. *Sensors and Actuators B: Chemical*, **348**:130662, 2021. DOI: https://doi.org/10.1016/j.snb.2021.130662.

[162] D. B. Christopher Leslee, B. Madheswaran, J. Gunasekaran, S. Karuppannan, and S. B. Kuppannan. Iminobenzophenone-thiophen hydrazide schiff base: a selective turn on sensor for paramagnetic Fe^{3+} ion and application in real sample analysis. *Photochemical & Photobiological Sciences*, **22**(8):1933–1943, 2023. DOI: https://doi.org/10.1007/s43630-023-00422-4.

[163] X. Sun, J. Zhang, X. Wang, J. Zhao, W. Pan, G. Yu, Y. Qu, and J. Wang. Colorimetric and fluorimetric dual mode detection of Fe^{2+} in aqueous solution based on a carbon dots/phenanthroline system. *Arabian Journal of Chemistry*, **13**(4):5075–5083, 2020. DOI: https://doi.org/10.1016/j.arabjc.2020.02.007.

[164] J. R. Bhamore, T. J. Park, and S. K. Kailasa. Glutathione-capped Syzygium cumini carbon dot-amalgamated agarose hydrogel film for naked-eye detection of heavy metal ions. *Journal of Analytical Science and Technology*, **11**:1–9, 2020. DOI: https://doi.org/10.1186/s40543-020-00208-8.

[165] W. Liu, L. Tian, J. Du, J. Wu, Y. Liu, G. Wu, and X. Lu. Triggered peroxidase-like activity of Au decorated carbon dots for colorimetric monitoring of Hg^{2+} enrichment in Chlorella vulgaris. *Analyst*, **145**(16):5500–5507, 2020. DOI: https://doi.org/10.1039/D0AN00930J.

[166] J. Pu, C. Liu, B. Wang, P. Liu, Y. Jin, and J. Chen. Orange red-emitting carbon dots for enhanced colorimetric detection of Fe^{3+}. *Analyst*, **146**(3):1032–1039, 2021. DOI: https://doi.org/10.1039/D0AN02075C.

[167] C. Lu, H. Ding, Y. Wang, C. Xiong, and X. Wang. Colorimetric and turn-on fluorescence determination of mercury (II) by using carbon dots and gold nanoparticles. *Nanotechnology*, **32**(15):155501, 2021. DOI: https://doi.org/10.1088/1361-6528/abd977.

[168] N. Singh, S. Kumari, and S. Khan. Naked eye colorimetric detection of fluoride through TiO_2 NPs/CQDs based detector. *Spectrochimica Acta Part A: Molecular and Biomolecular Spectroscopy*, **254**:119637, 2021. DOI: https://doi.org/10.1016/j.saa.2021.119637.

[169] J. An, R. Chen, M. Chen, Y. Hu, Y. Lyu, and Y. Liu. An ultrasensitive turn-on ratiometric fluorescent probes for detection of Ag^{+} based on carbon dots/SiO_2 and gold nanoclusters. *Sensors and Actuators B: Chemical*, **329**:129097, 2021. DOI: https://doi.org/10.1016/j.snb.2020.129097.

[170] N. Gogoi, M. Barooah, G. Majumdar, and D. Chowdhury. Carbon dots rooted agarose hydrogel hybrid platform for optical detection and separation of heavy metal ions. *ACS Applied Materials & Interfaces*, **7**(5):3058–3067, 2015. DOI: https://doi.org/10.1021/am506558d.

[171] H. Bai, Z. Tu, Y. Liu, Q. Tai, Z. Guo, and S. Liu. Dual-emission carbon dots-stabilized copper nanoclusters for ratiometric and visual detection of Cr2O72- ions and Cd^{2+} ions. *Journal of Hazardous Materials*, **386**:121654, 2020. DOI: https://doi.org/10.1016/j.jhazmat.2019.121654.

[172] Z. Li, S. Pang, M. Wang, M. Wu, P. Li, J. Bai, and X. Yang. Dual-emission carbon dots-copper nanoclusters ratiometric photoluminescent nano-composites for highly sensitive and selective detection of Hg^{2+}. *Ceramics International*, **47**(13):18238–18245, 2021. DOI: https://doi.org/10.1016/j.ceramint.2021.03.143.

[173] B. Peng, M. Fan, J. Xu, Y. Guo, Y. Ma, M. Zhou, J. Bai, J. Wang, and Y. Fang. Dual-emission ratio fluorescent probes based on carbon dots and gold nanoclusters for visual and fluorescent detection of copper ions. *Microchimica Acta*, **187**:1–9, 2020. DOI: https://doi.org/10.1007/s00604-020-04641-9.

[174] H. Guo, X. Wang, N. Wu, M. Xu, M. Wang, L. Zhang, and W. Yang. In-situ synthesis of carbon dots-embedded europium metal-organic frameworks for ratiometric fluorescence detection of Hg^{2+} in aqueous environment. *Analytica Chimica Acta*, **1141**:13–20, 2021. DOI: https://doi.org/10.1016/j.aca.2020.10.028.

[175] X. Guo, Q. Pan, X. Song, Q. Guo, S. Zhou, J. Qiu, and G. Dong. Embedding carbon dots in Eu3+-doped metal-organic framework for label-free ratiometric fluorescence detection of Fe^{3+} ions. *Journal of the American Ceramic Society*, **104**(2):886–895, 2021. DOI: https://doi.org/10.1111/jace.17477.

[176] J. Yang, B. Ruan, Q. Ye, L. C. Tsai, N. Ma, T. Jiang, and F. C. Tsai. Carbon dots-embedded zinc-based metal-organic framework as a dual-emitting platform for metal cation detection. *Microporous and Mesoporous Materials*, **331**:111630, 2022. DOI: https://doi.org/10.1016/j.micromeso.2021.111630.

[177] R. Long, C. Tang, T. Li, X. Tong, C. Tong, Y. Guo, Q. Gao, L. Wu, and S. Shi. Dual-emissive carbon dots for dual-channel ratiometric fluorometric determination of pH and mercury ion and intracellular imaging. *Microchimica Acta*, **187**:1–8, 2020. DOI: https://doi.org/10.1007/s00604-020-04287-7.

[178] Z. Chen, X. Xu, D. Meng, H. Jiang, Y. Zhou, S. Feng, Z. Mu, and Y. Yang. Dual-emitting N/S-doped carbon dots-based ratiometric fluorescent and light scattering sensor for high precision detection of Fe (III) ions. *Journal of Fluorescence*, **30**:1007–1013, 2020. DOI: https://doi.org/10.1007/s10895-020-02571-6.

[179] M. Jia, L. Peng, M. Yang, H. Wei, M. Zhang, and Y. Wang. Carbon dots with dual emission: A versatile sensing platform for rapid assay of Cr (VI). *Carbon*, **182**:42–50, 2021. DOI: https://doi.org/10.1016/j.carbon.2021.05.050.

[180] H. Chu, D. Yao, J. Chen, M. Yu, and L. Su. Detection of Hg^{2+} by a dual-fluorescence ratio probe constructed with rare-earth-element-doped cadmium telluride quantum dots and fluorescent carbon dots. *ACS Omega*, **6**(16):10735–10744, 2021. DOI: https://doi.org/10.1021/acsomega.1c00263.

[181] K. Jia, K. Yi, W. Zhang, P. Yan, S. Zhang, and X. Liu. Carbon nanodots calibrated fluorescent probe of QD@amphiphilic polyurethane for ratiometric detection of Hg (II). *Sensors and Actuators B: Chemical*, **370**:132443, 2022. DOI: https://doi.org/10.1016/j.snb.2022.132443.

[182] Z. Gan, X. Hu, X. Huang, Z. Li, X. Zou, J. Shi, W. Zhang, Y. Li, and Y Xu. A dual-emission fluorescence sensor for ultrasensitive sensing mercury in milk based on carbon quantum dots modified with europium (III) complexes. *Sensors and Actuators B: Chemical*, **328**:128997, 2021. DOI: https://doi.org/10.1016/j.snb.2020.128997.

[183] P. Lv, Y. Xu, Z. Liu, G. Li, and B. Ye. Carbon dots doped lanthanide coordination polymers as dual-function fluorescent probe for ratio sensing $Fe^{2+/3+}$ and ascorbic acid. *Microchemical Journal*, **152**:104255, 2020. DOI: https://doi.org/10.1016/j.microc.2019.104255.

[184] T. Watcharamongkol, P. Khaopueak, C. Seesuea, and K. Wechakorn. Green hydrothermal synthesis of multifunctional carbon dots from cassava pulps for metal sensing, antioxidant, and mercury detoxification in plants. *Carbon Resources Conversion*, **7**(2):100206, 2024. DOI: https://doi.org/10.1016/j.crcon.2023.100206.

[185] P. Krishnaiah, R. Atchudan, S. Perumal, E. S. Salama, Y. R. Lee, and B. H. Jeon. Utilization of waste biomass of Poa pratensis for green synthesis of n-doped carbon dots and its application in detection of Mn^{2+} and Fe^{3+}. *Chemosphere*, **286**:131764, 2022. DOI: https://doi.org/10.1016/j.chemosphere.2021.131764.

[186] O. J. Achadu, G. L. Elizur, T. E. Boye, and E. Y. Park. Green synthesis of carbon dots using expired agar for a label-free fluorescence signal-amplified detection of ferric ion utilizing oxalate functionalization. *Materials Advances*, **3**(15):6307–6315, 2022. DOI: https://doi.org/10.1039/D2MA00567K.

[187] J. Singh, S. Kaur, J. Lee, A. Mehta, S. Kumar, K. H. Kim, S. Basu, and M. Rawat. Highly fluorescent carbon dots derived from Mangifera indica leaves for selective detection of metal ions. *Science of the Total Environment*, **720**:137604, 2020. DOI: https://doi.org/10.1016/j.scitotenv.2020.137604.

[188] A. M. Senol and E. Bozkurt. Facile green and one-pot synthesis of seville orange derived carbon dots as a fluorescent sensor for Fe^{3+} ions. *Microchemical Journal*, **159**:105357, 2020. DOI: https://doi.org/10.1016/j.microc.2020.105357.

[189] A. Tadesse, M. Hagos, D. RamaDevi, K. Basavaiah, and N Belachew. Fluorescent-nitrogen-doped carbon quantum dots derived from citrus lemon juice: green synthesis, mercury (II) ion sensing, and live cell imaging. *ACS omega*, **5**(8):3889–3898, 2020. DOI: https://doi.org/10.1021/acsomega.9b03175.

[190] M. Wang, R. Shi, M. Gao, K. Zhang, L. Deng, Q. Fu, L. Wang, and D. Gao. Sensitivity fluorescent switching sensor for Cr (VI) and ascorbic acid detection based on orange peels-derived carbon dots modified with EDTA. *Food Chemistry*, **318**:126506, 2020. DOI: https://doi.org/10.1016/j.foodchem.2020.126506.

[191] G. Chellasamy, S. K. Arumugasamy, S. Govindaraju, and K. Yun. Green synthesized carbon quantum dots from maple tree leaves for biosensing of Cesium and electrocatalytic oxidation of glycerol. *Chemosphere*, **287**:131915, 2022. DOI: https://doi.org/10.1016/j.chemosphere.2021.131915.

[192] M. Zulfajri, K. C. Liu, Y. H. Pu, A. Rasool, S. Dayalan, and G. G. Huang. Utilization of carbon dots derived from Volvariella volvacea mushroom for a highly sensitive detection of Fe^{3+} and Pb^{2+} ions in aqueous solutions. *Chemosensors*, **8**(3):47, 2020. DOI: https://doi.org/10.3390/chemosensors8030047.

[193] T. Arumugham, M. Alagumuthu, R. G. Amimodu, S. Munusamy, and S. K. Iyer. A sustainable synthesis of green carbon quantum dot

(CQD) from Catharanthus roseus (white flowering plant) leaves and investigation of its dual fluorescence responsive behavior in multi-ion detection and biological applications. *Sustainable Materials and Technologies*, **23**:e00138, 2020. DOI: https://doi.org/10.1016/j.susmat.2019.e00138.

[194] N. Chaudhary, P. K. Gupta, S. Eremin, and P. R. Solanki. One-step green approach to synthesize highly fluorescent carbon quantum dots from banana juice for selective detection of copper ions. *Journal of Environmental Chemical Engineering*, **8**(3):103720, 2020. DOI: https://doi.org/10.1016/j.jece.2020.103720.

[195] R. Atchudan, T. N. J. I. Edison, S. Perumal, N. Muthuchamy, and Y. R. Lee. Hydrophilic nitrogen-doped carbon dots from biowaste using dwarf banana peel for environmental and biological applications. *Fuel*, **275**:117821, 2020. DOI: https://doi.org/10.1016/j.fuel.2020.117821.

[196] S. Zhao, X. Song, X. Chai, P. Zhao, H. He, and Z Liu. Green production of fluorescent carbon quantum dots based on pine wood and its application in the detection of Fe^{3+}. . *Journal of Cleaner Production*, **263**:121561, 2020. DOI: https://doi.org/10.1016/j.jclepro.2020.121561.

[197] G. Hu, L. Ge, Y. Li, M. Mukhtar, B. Shen, D. Yang, and J. Li. Carbon dots derived from flax straw for highly sensitive and selective detections of cobalt, chromium, and ascorbic acid. *Journal of Colloid and Interface Science*, **579**:96–108, 2020. DOI: https://doi.org/10.1016/j.jcis.2020.06.034.

[198] N. K. Sahoo, G. C. Jana, M. N. Aktara, S. Das, S. Nayim, A. Patra, P. Bhattacharjee, K. Bhadra, and M Hossain. Carbon dots derived from lychee waste: Application for Fe^{3+} ions sensing in real water and multicolor cell imaging of skin melanoma cells. *Materials Science and Engineering: C*, **108**:110429, 2020. DOI: https://doi.org/10.1016/j.msec.2019.110429.

[199] C. Zhao, X. Li, C. Cheng, and Y. Yang. Green and microwave-assisted synthesis of carbon dots and application for visual detection of cobalt (II) ions and pH sensing. *Microchemical Journal*, **147**:183–190, 2019. DOI: https://doi.org/10.1016/j.microc.2019.03.029.

[200] A. K. Singh, V. K. Singh, M. Singh, P. Singh, S. R. Khadim, U. Singh, B. Koch, S. Hasan, and R. Asthana. One pot hydrothermal synthesis of fluorescent NP-carbon dots derived from Dunaliella salina biomass and its application in on-off sensing of Hg (II), Cr (VI) and live cell imaging. *Journal of Photochemistry and Photobiology A: Chemistry*, **376**:63–72, 2019. DOI: https://doi.org/10.1016/j.jphotochem.2019.02.023.

[201] M. Zulfajri, G. Gedda, C. J. Chang, Y. P. Chang, and G. G. Huang. Cranberry beans derived carbon dots as a potential fluorescence sensor for selective detection of Fe^{3+} ions in aqueous solution. *ACS omega*, **4**(13):15382–15392, 2019. DOI: https://doi.org/10.1021/acsomega.9b01333.

[202] J. Plácido, S. Bustamante-López, K. Meissner, D. Kelly, and S. Kelly. Microalgae biochar-derived carbon dots and their application in heavy metal sensing in aqueous systems. *Science of the Total Environment*, **656**:531–539, 2019. DOI: https://doi.org/10.1016/j.scitotenv.2018.11.393.

[203] N. Pourreza and M. Ghomi. Green synthesized carbon quantum dots from Prosopis juliflora leaves as a dual off-on fluorescence probe for sensing mercury (II) and chemet drug. *Materials Science and Engineering: C*, **98**:887–896, 2019. DOI: https://doi.org/10.1016/j.msec.2018.12.141.